Diploma Thesis

Vibrational aspects of Graphene and related two dimensional materials

Heraklio 2014

by

MARIA SEVASTAKI

msevastaki@gmail.com

3425

Department of Physics
University of Crete

Acknowledgments

First, I would like to thank my supervisor, Giorgos Tsironis, for introducing me into the Condensed Matter Physics and giving me the opportunity to work on such a fascinating subject as the vibrational aspects of graphene and related two dimensional materials.
I am grateful for his guidance, encouragement and trust during this work.

I feel very grateful to my colleagues, the people I worked with during my stay in Professor Tsironis' group. Particularly, Alberto Fraile, Nikos Lazarides, Marios Mattheakis, Joniald Shena, Thomas Oikonomou, Kyriakos Skoufaris, Margaris Ioannis and Konstantinos-Othon Chatzibaloglou were always there to listen and help me with my Diploma Thesis giving me advices.

I also want to thank all my friends for their friendship and support. I won't refer to them by name, but they will know when they read. Although they haven't realized it, their contribution in this Thesis was essential.

This Diploma Thesis would not have been completed in time if my great friend, Sailing coach and head of Education Team Computer Center at University of Crete, George Vitsakis, had not provided me with the necessary computing power.

Last but not least, I would like to thank my family: my parents, George and Kathrin, for being always next to me, helping me and supporting me, even when I turned to be a great trouble, and my sister and brother, Christine and Hercules, for cheering me up when I had bad time.

I. INTRODUCTION

1. Graphene

Graphene has been a rapidly rising star on the horizon of materials science and condensed matter physics [1]. Since the extraction from graphite, the monatomic layer of carbon atoms arranged into a two-dimensional hexagonal lattice, called graphene, has become a hot topic in science because it is promising for many applications. The physical properties of graphene, such as thermal conductivity, optical conductivity, electron spectrum, phonon vibrations, elastic properties and sound velocities can be tuned in a controllable way by applying elastic strain. The stability range of flat graphene in the three-dimensional space of the plane strain components was reported in [2].

As a defect-free material, graphene is predicted to have an intrinsic tensile strength higher than any other known material and tensile stiffness similar to values measured for graphite [3]. Graphene is a nanosized carbon polymorph and has drawn a great deal of attention due to its unique physical properties, which can be used in electronics, optics, spintronics, hydrogen transportation and storage, composite materials and many other fields. The physical and mechanical properties of graphene change noticeably depending on the applied deformation, which makes it possible to improve its useful properties [4].

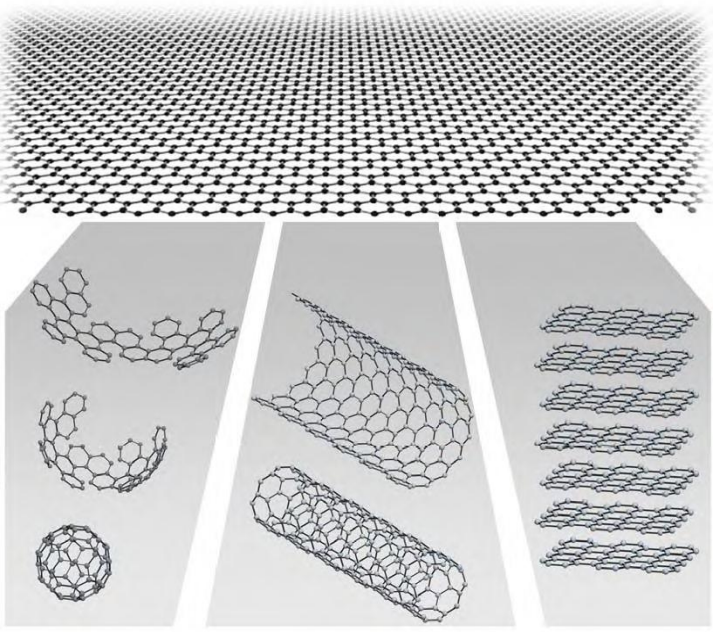

Figure 1: Graphene is a 2D material. It can be wrapped up into 0D buckyballs, rolled into 1D nanotubes or stacked into 3D graphite [1].

Graphene is the name given to a flat monolayer of carbon atoms tightly packed into a two-dimensional (2D) honeycomb lattice, and is a basic building block for graphitic materials of all other dimensionalities (Figure 1). It can be wrapped up into 0D fullerenes, stacked into 3D graphite or rolled into 1D nanotubes [1, 3].

Theoretically, graphene has been studied for many years and widely used for describing properties of various carbon-based materials. Graphene was known as integral part of 3D materials and was presumed not to exist in the free state, being described as an “academic” material. Also they believed to be unstable with respect to the formation of curved structures, fullerenes and nanotubes [1]. Suddenly, free-standing graphene was found ten years ago [5]

The following are a few words about the history of Graphene. More than 70 years ago, Landau and Peierls [6, 7] argued that strictly two-dimensional (2D) crystals were thermodynamically unstable and could not exist. Their theory pointed out that a divergent contribution of thermal fluctuations in low-dimensional crystal lattices should lead to such displacements of atoms that they become comparable to interatomic distances at any finite temperature. The argument was later extended by Mermin [8] and is strongly supported by a whole omnibus of experimental observations. Indeed, the melting temperature of thin films rapidly decreases with decreasing thickness, and they become unstable (segregate into islands or decompose) at a thickness of, typically, dozens of atomic layers. For this reason, atomic monolayers have so far been known only as an integral part of larger 3D structures, usually grown epitaxially on top of monocrystals with matching crystal lattices [1]. Without such a 3D base, 2D materials were presumed not to exist until 2004, when the common wisdom was flaunted by the experimental discovery of graphene [5] and other free-standing 2D atomic crystals (for example, single-layer boron nitride). These crystals could be obtained on top of non-crystalline substrates, in liquid suspension and as suspended membranes.

Importantly, the 2D crystals were found not only to be continuous but to exhibit high crystal quality [1, 5]. The latter is most obvious for the case of graphene, in which charge carriers can travel thousands interatomic distances without scattering [1, 5]. With the benefit of hindsight, the existence of such one-atom-thick crystals can be reconciled with theory. Indeed, it can be argued that the obtained 2D crystallites are quenched in a metastable state because they are extracted from 3D materials, whereas their small size (<<1mm) and strong interatomic bonds assure that thermal fluctuations cannot lead to the generation of dislocations or other crystal defects even at elevated temperature [1].

2. Boron Nitride (BN)

Boron nitride is a chemical compound with chemical formula BN, consisting of equal numbers of boron and nitrogen atoms [9]. BN is isoelectronic to a similarly structured carbon lattice and thus exists in various crystalline forms. The hexagonal form corresponding to graphite is the most stable and softest among BN polymorphs, and is therefore used as a lubricant and an additive to cosmetic products. The cubic (sphalerite structure) variety analogous to diamond is called c-BN. Its hardness is inferior only to diamond, but its thermal and chemical stability is superior. The rare wurtzite BN modification is similar to lonsdaleite and may even be harder than the cubic form [10].

Boron nitride has also potential use in nanotechnology. Nanotubes of BN can be produced that have a structure similar to that of carbon nanotubes, i.e. graphene (or BN) sheets rolled on themselves but the properties are very different.

The most stable crystalline form is the hexagonal one, also called h-BN, α-BN, or g-BN (graphitic BN). It has a layered structure similar to graphite. Within each layer, boron and nitrogen atoms are bound by strong covalent bonds, whereas the layers are held together by weak van der Waals forces. The interlayer "registry" of these sheets differs, however, from the pattern seen for graphite, because the atoms are eclipsed, with boron atoms lying over and above nitrogen atoms. This registry reflects the polarity of the B-N bonds. Still, h-BN and graphite are very close neighbors and even the BC_6N hybrids have been synthesized where carbon substitutes for some B and N atoms [11].

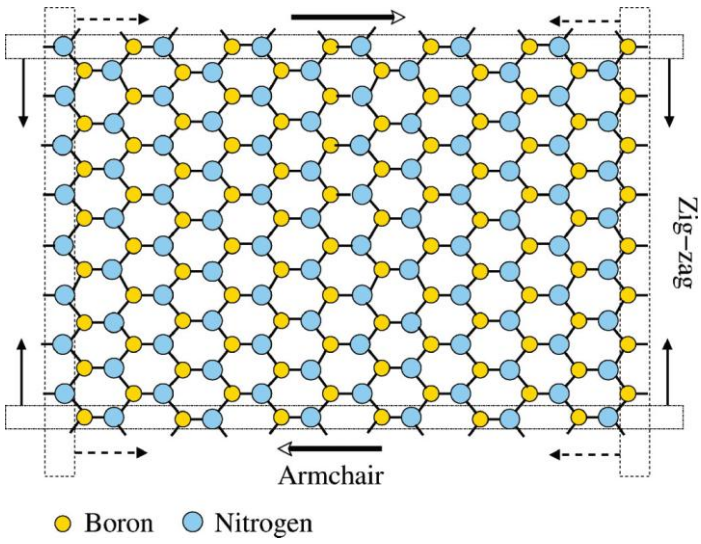

Figure 2: The h-BN sheet. Yellow (Blue) circles refer to the B (N) atoms.

A single layer of hexagonal boron-nitride (h-BN) is a wide gap insulator that is very promising for optoelectronic technologies, tunnel devices, and field-effect transistors.

BN has excellent thermal and chemical stability. Because of this, boron nitride ceramics are used as parts of high-temperature equipment. h-BN can be included in ceramics, plastics, rubbers, alloys, resins, and other materials. Such materials are suitable for construction of e.g. bearings and in steelmaking [12]. Plastics filled with BN have less thermal expansion as well as higher thermal conductivity and electrical resistivity. Due to its excellent dielectric and thermal properties, BN is used in electronics e.g. as a substrate for semiconductors, microwave-transparent windows, and as a structural material for seals [13].

Hexagonal BN is used in laser printers as a charge leakage barrier layer of the photo drum [14]. In the automotive industry, h-BN mixed with a binder (boron oxide) is used for sealing oxygen sensors, which provide feedback for adjusting fuel flow. The binder utilizes the unique temperature stability and insulating properties of h-BN [12].

And now a few words about graphene, BN stability and mixtures of BN with carbon. According to the Mermin-Wagner [15] theorem, the stability of any two-dimensional crystal is only possible in the presence of atomic corrugations which distort the perfect honeycomb lattice and allow the atoms to explore the out-of plane direction. Experimental observations have found ripples in suspended sheets of graphene, and atomistic simulations suggest that the strong bonds between the carbon atoms determine the features of these ripples. Understanding the behavior of the ripples is important for many reasons. They affect the electronic transport properties, e.g., in GE the ripples are believed to be one of the dominant scattering sources which limits the electron mobility. h-BN ribbons doped by carbon have recently been proposed.

In addition, BN based nanostructures are potential materials for thermal management applications because of their high thermal conductivity and sensitivity to isotopic substitution, etc [9].

3. Breathers

Discrete breathers (DB) which also called intrinsic localized modes (ILM) or discrete solitons appears in strongly nonlinear systems [16]. They have been identified as exact solutions to a number of model nonlinear systems possessing translational symmetry [17]. DB was reported for the first time in 1988, is a time-periodic and spatially localized vibration mode that appears in a lattice system that consists of discrete elements under nonlinear interactions [18]. Since then the role of DBs has been extensively discussed in relation to many physical systems [2, 4, 16-18].

Diversity of physical systems supporting DBs suggests that they are very common in nonlinear lattices. Crystals are natural nonlinear lattices and many studies, both experimental and numerical, have been done to prove the existence of DBs and to use them for explanation of various physical effects in crystals [17]. According to computer simulations, DBs can also be excited in graphene [4, 18]. Linear and nonlinear vibrational modes can exist at the edges of graphene nanoribbons and in other carbon nanopolymorphs [2].

Both the discreteness and the nonlinearity of the system excite the ILM. First of all, waves with a frequency exceeding the upper bound of phonon band ω_{max} cannot disperse in the system that consists of discrete elements. Also some nonlinear waves can vibrate with a frequency higher than ω_{max}, although they cannot spread. Finally the nonlinearity in the interaction between the elements tends to excite waves with relatively large amplitude.

Adding to this, the ILM is observed experimentally in real systems, such as Josephson junction arrays, optical lattices and micromechanical cantilever arrays [16, 18]. Although these are not atomic systems, the ILM is also expected in atomic systems because of the discreteness of their structures and the nonlinearity of interaction between atoms. As a result, the excitation of the ILM is expected in a crystal structure. Although, for the sake of simplicity, most studies on the ILM have dealt with one-dimensional lattice systems, a crystal consisting of regularly arranged discrete atoms with nonlinear interactions is one candidate in which the ILM may develop. One of the possible extensions is the consideration of higher-dimensional systems. In particular, the ILM has been observed theoretically in various two-dimensional systems as we will see later [18].

4. Molecular Dynamics

Molecular Dynamics (MD) simulation is a technique to compute the equilibrium and transport properties of a classical many-body system. In this context, the word classical means that the nuclear motion of the constituent particles obeys the laws of classical mechanics. This is an excellent approximation for a wide range of materials [19].

In a MD simulation, the classical equations of motion governing the microscopic time evolution of a many-body system are solved numerically subject to boundary conditions appropriate for the geometry or symmetry of the system. Thus, MD methodology is founded upon the basic principles of classical mechanics and can provide a window into the microscopic dynamical behavior of the individual atoms that make up a given system. In order to provide a picture of the microscopic behavior of a system from the laws of classical mechanics, MD requires, as an input, a description of the interparticle interactions. The quality of the results of an MD simulation depends on the accuracy of this description [20].

Only when we consider translational or rotational motion of light atoms or molecules or vibrational motion with a frequency ν such that $h\nu > k_B T$, should we worry about quantum effects. MD simulations are in many respects very similar to real experiments and can help to understand experimental results [19].

The classical motion of the system is determined by Newton's second law:

$$m_i \ddot{r}_i = F_i \tag{1}$$

Where: m_i are the masses

r_i are the velocities

And F_i are the forces

Now we need to recast the Newton's second law to Hamiltonian form. The Hamiltonian for an N-particle system subject only to interparticle interactions is:

$$H(p,r) \equiv H(p_i, \dots, p_N, r_i, \dots, r_N) = \sum_{i=1}^{N} \frac{{p_i}^2}{2m_i} + U(r_i, \dots, r_N) \tag{2}$$

Where $p_i, \dots, p_N$ are the momenta of the particles defined by $p_i = m_i v_i$ and $U(r_i, \dots, r_N)$ is the interparticle potential, in terms of which the force are given by

$$F_i = -\frac{\partial U}{\partial r_i} \tag{3}$$

The (1) can be derived from (2) according to Hamiltonian's equation

$$\dot{r_i} = \frac{\partial H}{\partial p_i} = \frac{p_i}{m_i} \tag{4}$$

$$\dot{p_i} = -\frac{\partial H}{\partial r_i} = -\frac{\partial U}{\partial r_i} = F_i(r_i, \dots, r_N) \tag{5}$$

The conservation of the Hamiltonian is equivalent to the conservation of the total energy of the system and provides an important link between molecular dynamics and statistical mechanics. Statistical mechanics is based on the Gibbs' ensemble concept. That is, many individual microscopic configurations of a very large system lead to the same macroscopic properties, implying that it is not necessary to know the precise detailed motion of every particle in a system in order to predict its properties. Statistical ensembles are usually characterized by fixed values of thermodynamic variables such as energy (E), temperature (T), pressure (P), volume (V), particle number (N) or chemical potential (μ). One fundamental ensemble is called the microcanonical ensemble and is characterized by constant particle number (N), constant volume (V), and constant total energy (E) and is denoted as the NVE ensemble. Other examples include the canonical or NVT ensemble, the isothermal-isobaric or NPT ensemble, and the grand canonical or μVT ensemble [20].

MD studies relay on the quality of interatomic potentials, which is always a question. In this study the molecular dynamics simulation of DBs in graphene was performed using the LAMMPS package. The name LAMMPS came from Large-scale Atomic/Molecular Massively Parallel Simulator. It is distributed as an open source code and also can be used in single and parallel processors.

5. Literature Review

Four previous papers are being used as guide to our work. In chronological order they are: First, "Excitation of localized modes in a graphene sheet" [18]. Secondly, "Discrete Breathers in Deformed Graphene" [4], "Discrete breather clusters in strained graphene" [2] and the most recent "Properties of discrete breathers in graphene from *ab initio* simulations" [17].

In the first paper they analyzed the two-dimensional vibration of a graphene sheet using MD simulations and discussed the possibility of ILM excitation in a real material. They used Brenner potential [25] and they made MD simulations with a sample containing 336 carbon atoms. Also they created DBs with the following method. An initial displacement is applied to six atoms as shown in the Figure 3.

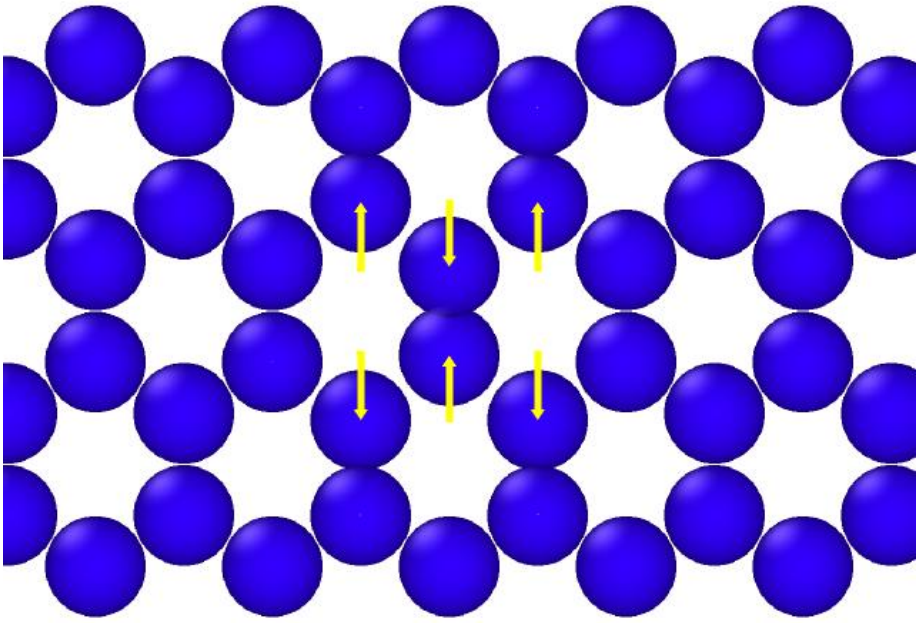

Figure 3. Schematic illustration of the initial condition to generate ILMs. (Yellow arrows are not a scale).

They observed some characteristic features of the ILM. The size of the energy localization was two atoms and it was observed in a few regions. Also they observed fairly constant vibration modes, in which the two neighboring atoms vibrated in the opposite direction. Furthermore the frequency of the localized vibration exceeded the upper bound of the phonon band and the mode was similar to one of the linear eigenmodes.

Finally the localized vibration continued for a fairly long time (26 cycles), which indicates the excitation of the ILM in the graphene sheet.

In the second paper [4], the graphene dynamics was studied on the atomic level using again the many-body interatomic potential (Brenner potential) and they discovered new DBs, the frequency of which was located in the spectrum but they were not embedded. The simulations were carried out in samples with 32 x 35 unit cells which means 2048 carbon atoms.

For the study of the DBs they used an external force. This force was applied to two atoms to increase the oscillation amplitude. The force acted on the atoms only when they moved to the equilibrium positions. The action of the external force was stopped when the desired amplitude of the DB was reached. The frequency of the DB was varied between 27 and 32 THz and the lifetime was 900 oscillation periods. They found that the phonon density of states (PhDOS) of undeformed graphene, as well as the phonon spectrum of graphene under the action of the hydrostatic deformation, had no gap. The gap in the phonon spectrum appeared at the uniaxial deformation along the armchair or zigzag direction [4]. The importance of the gap in the PhDOS is also stressed in the [4].

In the third paper [2] also by means of MD simulations, they studied the properties of DB clusters in a graphene sheet which was subjected to homogeneous elastic strain in order to introduce a gap into the phonon spectrum. Several DB clusters containing up to four DBs were investigated.
They used their own (Tersoff-like) potential which described in [21] and they made simulations with 50 x 50 primitive cells which means 5000 carbon atoms. The graphene lattice was elastically strained and the stability of the DB clusters was checked by introducing small perturbations.

The frequency of the DB in this paper ranged from 25 to 30 THz. Also they noted that for the considered values of strain, the DB cannot have amplitude larger than 0.7 Å and smaller than 0.2 Å.
So they show that the PhDOS of unstrained graphene does not have gaps and this precludes the existence of gap DBs.
The effect of the energy exchange between DBs in DB clusters was observed. DB clusters are interesting because they can localized a larger amount of energy than a single DB [2].

In the last paper [17] DB in graphane (two-dimensional polymer of carbon and hydrogen with the formula unit $(CH)_n$) has been studied with the aid of *ab initio* calculations and they compared the results with those using the AIREBO interatomic potential. DB was used to explain basic physics behind the dehydrogenation kinetics of graphane at finite temperatures.
The DB is created adding an out of plane displacement to one H atom but as we will see the same can not be done in pure graphene.

DBs in graphane demonstrate the soft-type anharmonicity with frequency monotonously decreasing with increasing amplitude. On the other hand, MD simulations based on the AIREBO potential give an adequate description of the $\omega_{DB}(A)$ curve only for small amplitudes and fail for large amplitudes.

Table 1: Summary of the literature review about DBs. Potentials, parameters of the simulations and main results.

	Potential	Simulation cell (N of atoms)	Lifetime (ps)	Frequency (THz)
Y.Yamayose[18]	Brenner	336	1	~50
L. Z. Khadeeva[4]	Their own (Tersoff-like)	2048	29.7	27-32
J. A. Baimova[2]	Their own (Tersoff-like)	5000	0.5 to 10	25-30
G.M.Chechin[17]	AIREBO ab initio	32 carbon and 32 hydrogen	1.75	35-80

6. Interatomic potentials

In this section we will refer to the potentials used in this work. For the simulations we use the following three potentials Tersoff, AIREBO and LCBOP.

Tersoff

First we will describe the Tersoff potential that as we will see is somewhere the basis of the other two. The form Tersoff [22, 23] used in this study can be written as:

$$V_{ij} = f_C(r_{ij})\left[f_R(r_{ij}) + b_{ij} f_A(r_{ij})\right] \quad (1)$$

Where: f_C is a cutoff term to guarantee first nearest-neighbor interaction.

$$f_C(r) = \begin{cases} 1 & : \quad r < R - D \\ \frac{1}{2} - \frac{1}{2}\sin\left(\frac{\pi}{2}\frac{r-R}{D}\right) & : R - D < r < R + D \\ 0 & : \quad r > R + D \end{cases} \quad (2)$$

f_R is a two-body term

$$f_R(r) = Aexp(-\lambda_1 r) \quad (3)$$

f_A includes three-body interactions

$$f_A(r) = -Bexp(-\lambda_2 r) \quad (4)$$

And b_{ij} is the bond angle term which depends on the local coordination of atoms around atom *i* and the angle between atoms *i*, *j* and *k* (θ_{ijk}).

$$b_{ij} = \left(1 + \beta^n \zeta_{ij}^n\right)^{-\frac{1}{2n}} \quad (5)$$

With

$$\zeta_{ij} = \sum_{k \neq i,j} f_C(r_{ik}) g(\theta_{ijk}) exp\left[\lambda_3^3 (r_{ij} - r_{ik})^3\right] \quad (6)$$

And

$$g(\theta) = \left(1 + \frac{c^2}{d^2} - \frac{c^2}{[d^2 + (\cos\theta - h)^2]}\right) \quad (7)$$

The summation in the formula is over all neighbors *j* and *k* of atom *i* within a cutoff distance equal to *R* + *D*.

The energy computed as:

$$E = \frac{1}{2}\sum_i \sum_{j \neq i} V_{ij} \quad (8)$$

AIREBO

We will start with the REBO potential. REBO uses a Tersoff-style potential to describe the covalent bonding interactions in carbon and hydrocarbon systems. The REBO potential had been extended to provide more accurate treatment of the energetic, elastic, and vibrational properties of solid carbon and small hydrocarbons. Also this potential had been used to model many different materials and processes, including fullerenes, carbon nanotubes and amorphous carbon. On the other hand REBO is not appropriate for studying energy hydrocarbon systems because of the absence of dispersion and nonbonded repulsion terms. Various attempts have been made previously to combine nonbonded interactions with the Tersoff or REBO potentials in a way that preserves the reactive capabilities of the model. The new potential is the adaptive intermolecular REBO potential (AIREBO) [24, 25].

AIREBO potential is given by the expression:

$$E = \frac{1}{2}\sum_i \sum_{j \neq i} \left[E_{ij}^{REBO} + E_{ij}^{LJ} + \sum_{k \neq i,j} \sum_{l \neq i,j,k} E_{kijl}^{tors}\right] \quad (9)$$

Where: $$E_{ij}^{REBO} = V_{ij}^{R} + b_{ij} V_{ij}^{A} \quad (10)$$

And repulsive term is: $$V_{ij}^{R} = w_{ij}(r_{ij}) \left[1 + \frac{Q_{ij}}{r_{ij}}\right] A_{ij} e^{-a_{ij} r_{ij}} \quad (11)$$

The bond- weighting factor is: $$w_{ij}(r_{ij}) = S'\left(t_C(r_{ij})\right) \quad (12)$$

The switching function is:

$$S'^{(t)} = \Theta(-t) + \Theta(t)\Theta(1-t)\frac{1}{2}[1 + \cos(\pi t)] \quad (13)$$

With scaling function: $$t_C(r_{ij}) = \frac{r_{ij} - r_{ij}^{min}}{r_{ij}^{max} - r_{ij}^{min}} \quad (14)$$

And the attractive term i $$V_{ij}^{A} = -w_{ij}(r_{ij}) \sum_{n=1}^{3} B_{ij}^{(n)} e^{-\beta_{ij}^{(n)} r_{ij}} \quad (15)$$

Bond order for the interaction between atoms i and j

$$b_{ij} = \frac{1}{2}\left[p_{ij}^{\sigma\pi} + p_{ji}^{\sigma\pi}\right] + \pi_{ij}^{rc} + \pi_{ij}^{dh} \quad (16)$$

$p_{ij}^{\sigma\pi}$ is not necessarily equal to $p_{ji}^{\sigma\pi}$. The $p_{ij}^{\sigma\pi}$ term depends on the bond angles θ_{jik} between the $\mathbf{r}_{ji}$ vector and the vectors $\mathbf{r}_{ki}$ to any other neighboring atoms.

$$p_{ij}^{\sigma\pi} = \left[1 + \sum_{k\neq i,j} w_{ik}(r_{ik}) g_i\left(\cos\theta_{jik}\right) e^{\lambda_{jik}} + P_{ij}\right]^{-1/2} \quad (17)$$

The penalty function g_i imposes a cost on bonds that are too close to one another. Its functional form is a fifth-order spline. The penalty function g_i is:

$$g_C\left(\cos\theta_{jik}\right) = g_C^{(1)}\left(\cos\theta_{jik}\right) + S'\left(t_N\left(N_{ij}\right)\right)\left[g_C^{(2)}\left(\cos\theta_{jik}\right) - g_C^{(1)}\left(\cos\theta_{jik}\right)\right] \quad (18)$$

When the central atom is a carbon, the spline also depends on the local coordination number, defined as the sum of the carbon-only and hydrogen-only coordination numbers

$$N_{ij} = N_{ij}^{C} + N_{ij}^{H} \quad (19)$$

And $$N_{ij}^{C} = \left(\sum_{k\neq i} \delta_{kC} w_{ik}(r_{ik})\right) - \delta_{jC} w_{ij}\left(r_{ij}\right) \quad (20)$$

Also scaling function is: $$t_N\left(N_{ij}\right) = \frac{N_{ij} - N_{ij}^{min}}{N_{ij}^{max} - N_{ij}^{min}} \quad (21)$$

The two remaining terms, $e^{\lambda_{jik}}$ and P_{ij} are small correction factors. The $e^{\lambda_{jik}}$ term is added to improve the potential energy surface for abstraction of hydrogen atoms from hydrocarbons with

$$\lambda_{jik} = 4\delta_{iH}\left[\left(\delta_{kH}\rho_{HH} + \delta_{kC}\rho_{CH} - r_{ik}\right) - \left(\delta_{jH}\rho_{HH} + \delta_{jC}\rho_{CH} - r_{ij}\right)\right] \quad (22)$$

And P_{ij} is a two-dimensional cubic spline.

π_{ij}^{dh} imposes a penalty for rotation around multiple bonds.

$$\pi_{ij}^{dh} = T_{ij}\left(N_{ij}, N_{ji}, N_{ij}^{conj}\right) \sum_{k\neq i,j} \sum_{l\neq i,j} \left(1 - \cos^2\omega_{kijl}\right) \times w'_{ik}(r_{ik}) w'_{jl}(r_{jl}) \Theta\left(\sin\left(\theta_{jik}\right) - s^{min}\right) \times \Theta\left(\sin\left(\theta_{ijl}\right) - s^{min}\right) \quad (23)$$

T_{ij} is another three-dimensional cubic spline.

Local measure of conjugation in the i-j bond equal to:

$$N_{ij}^{conj} = 1 + \left[\sum_{k\neq i.j} \delta_{kC} w_{ik}(r_{ik}) S'\left(t_{conj}(N_{ki})\right)\right]^2 + \left[\sum_{l\neq i.j} \delta_{iC} w_{jl}(r_{jl}) S'\left(t_{conj}(N_{lj})\right)\right]^2 \quad (24)$$

With $t_{conj}(N)$ specifying the range of coordination numbers under

$$t_{conj}(N) = \frac{N - N^{min}}{N^{max} - N^{min}} \quad (25)$$

The torsion angle ω_{kijl} is defined in the usual way as the angle between the plane defined by the vectors $\mathbf{r}i_k$ and $\mathbf{r}_{ij}$ and that defined by $\mathbf{r}_{ij}$ and $\mathbf{r}_{jl}$

$$\cos\omega_{kijl} = \frac{r_{ji}\times r_{ik}}{|r_{ji}\times r_{ik}|} \cdot \frac{r_{ij}\times r_{jl}}{|r_{ij}\times r_{jl}|} \quad (26)$$

The bond-weighting function is: $$w'_{jl}(r_{jl}) = S' t'_C(r_{ij}) \quad (27)$$

With scaling function: $$t'_C(r_{ij}) = \frac{r_{ij} - r_{ij}^{min}}{r_{ij}^{max} - r_{ij}^{min}} \quad (28)$$

The Lennard-Jones (LJ) potential is:

$$E_{ij}^{LJ} = S\left(t_r(r_{ij})\right) S\left(t_b(b_{ij}^*)\right) C_{ij} V_{ij}^{LJ}(r_{ij}) + \left[1 - S\left(t_r(r_{ij})\right)\right] C_{ij} V_{ij}^{LJ}(r_{ij}) \quad (29)$$

With $V_{ij}^{LJ}(r_{ij})$ equal to: $$V_{ij}^{LJ}(r_{ij}) = 4\epsilon_{ij}\left[\left(\frac{\sigma_{ij}}{r_{ij}}\right)^{12} - \left(\frac{\sigma_{ij}}{r_{ij}}\right)^{6}\right] \quad (30)$$

And S(t) is an universal switching function,

$$S(t) = \Theta(-t) + \Theta(t)\Theta(1-t)[1 - t^2(3-2t)] \quad (31)$$

With scaling function: $$t_r(r_{ij}) = \frac{r_{ij} - r_{ij}^{LJ\,min}}{r_{ij}^{LJ\,max} - r_{ij}^{LJ\,min}} \quad (32)$$

At intramolecular distances, the LJ interaction is included only if there is no significant bonding interaction between the two atoms, as specified by the t_b switch:

$$t_b(b_{ij}) = \frac{b_{ij} - b_{ij}^{min}}{b_{ij}^{max} - b_{ij}^{min}} \quad (33)$$

And if the atoms *i* and *j* are not connected by two or fewer intermediate atoms. This latter switch is controlled by bond weights

$$C_{ij} = 1max\{w_{ij}(r_{ij}), \quad w_{ik}(r_{ik})w_{kj}(r_{kj}), \forall\, k \quad w_{ik}(r_{ik})w_{kl}(r_{kl})w_{lj}(r_{lj}), \forall k, l\} \tag{34}$$

The torsional potential is: $E_{kijl}^{tors} = w_{ki}(r_{ki})w_{ij}(r_{ij})w_{jl}(r_{jl})V^{tors}(\omega_{kijl})$ (35)

Where $$V^{tors}(\omega_{kijl}) = \frac{256}{405}\epsilon_{kijl}\cos^{10}\left(\omega_{kijl}/_2\right) - \frac{1}{10}\epsilon_{kijl} \tag{36}$$

LCBOP

The long-range carbon bond order potential (LCBOP) is based on an alternative approach: they exclude long-range interactions only for nearest neighbors and parametrize the short-range part of the potential in such a way that the combined potential yields the correct properties. Instead of the LJ potential the long-range potential is a Morse like potential which is based on a best fit of the interlayer interaction energy in graphite for a range of interplanar distances [26].

According to the LCBOP the energy given by:

$$E_b = \frac{1}{2}\sum_{i,j}^{N} V_{ij}^{tot} = \frac{1}{2}\sum_{i,j}^{N}\left(f_{c,ij}V_{ij}^{SR} + S_{ij}V_{ij}^{LR}\right) \tag{37}$$

Where: $$S_{ij} = 1 - f_{c,ij} \tag{38}$$

The short-range part is: $$V_{ij}^{SR} = V_R(r_{ij}) - B_{ij}V_A(r_{ij}) \tag{39}$$

Where: $$V_R(r) = Aexp(-ar) \tag{40}$$

And $$V_A(r) = B_1 exp(-\beta_1 r) + B_2 exp(-\beta_2 r) \tag{41}$$

The smooth cutoff function is: $$f_{c,ij} \equiv f_c(r_{ij}) \tag{42}$$

$$f_c(x) = \Theta(-x) + \Theta(x)\Theta(1-x)exp\left(\frac{\gamma x^3}{x^3-1}\right) \tag{43}$$

The parameter γ used to optimize the shape of the energy barrier for the diamond to graphite transformation.

Brenner function is: $$B_{ij} = \frac{1}{2}\left[b_{ij} + b_{ji} + F^{conj}\left(N_{ij}, N_{ji}, N_{ij}^{conj}\right)\right] \tag{44}$$

The angular dependent part is:

$$b_{ij} = \left(1 + \sum_{k \neq i,j} f_C(r_{ik}) G\left(\cos\theta_{ijk}\right) H\left(\delta r_{ijk}\right)\right)^{-\delta} \quad (45)$$

Where θ_{ijk} is the bond angle between the bonds ij and ik and δr_{ijk} is the difference in bond distance between these two bonds.

The $H\left(\delta r_{ijk}\right)$ optimize elastic properties, surface properties and the energy barrier for the diamond to graphite transformation.

$$H(x) = \begin{cases} H_1(x) = L\left(1 + k(x+d)\left(\frac{1}{1+[k(x+d)]^{10}}\right)^{1/10}\right), x < -d \\ H_2(x) = 1 + C_1 x + \frac{1}{2}C_1^2 x^2 + C_4 x^4 + C_6 x^6, -d \leq x \leq d \\ H_3(x) = R_0 + R_1(x-d), x > d \end{cases} \quad (46)$$

Where d is a fit parameter.

The coordination of atom i, N_i is: $N_i = \sum_k f_{c,ik}$ (47)

And $N_{ij} = min\left(3, \sum_{k \neq j} f_{c,ik}\right) = min\left(3, N_i - f_{c,ij}\right)$ (48)

And

$$N_{ij}^{conj} = \frac{(N_{ij}+1)(N_{ji}+1)\left(N_{ij}^{el}+N_{ij}^{el}\right)-4(N_{ij}+N_{ji}+2)}{N_{ij}(3-N_{ij})(N_{ji}+1)+N_{ji}(3-N_{ji})(N_{ij}+1)+\epsilon} \quad (49)$$

Where ϵ is a very small positive number and the N_{ij}^{el} gives the contribution of electrons from atom I to the bond ij.

$$N_{ij}^{el} = \frac{4-M_{ij}}{N_{ij}+1-M_{ij}} \quad (50)$$

With $M_{ij} = min\left(3, \widetilde{M_{ij}}\right)$ (51)

$$\widetilde{M_{ij}} = \sum_{k \neq i,j} f_{c,ik} F(x_{ik}) \quad (52)$$

$$x_{ik} = N_k - f_{c,ik} \quad (53)$$

And

$$F(x_{ik}) = \Theta(x_{ik} - 3) + \frac{1}{2}\Theta(x_{ik} - 2)\Theta(3 - x_{ik}) \times (1 - \cos[\pi(x_{ik} - 2)]) \quad (54)$$

So

$$F^{conj}\left(N_{ij}, N_{ji}, N_{ij}^{conj}\right) = \left(1 - N_{ij}^{conj}\right)F_0^{conj}\left(N_{ij}, N_{ji}\right)$$

$$+N_{ij}^{conj}F_1^{conj}\left(N_{ij}, N_{ji}\right) \quad (55)$$

The long-range part is calculated from the interplanar interaction energy in hexagonal graphite

$$E_l(d_l) = \frac{1}{2}\sum_i'\sum_j' f_{c,ij}^{LR}V_{ij}^{LR}\left(r_{ij}\right) \quad (56)$$

And $$V^{LR}(r) = \theta(r_0 - r)V_1^M(r) + \theta(r - r_0)V_2^M(r) \quad (57)$$

Where $$V_i^M(r) = \epsilon_i\left(e^{-2\lambda_i(r-r_0)} - 2e^{-\lambda_i(r-r_0)}\right) + u_i \quad (58)$$

is the Morse function.

As a conclusion of this short review the main difference between the potentials discussed before has to be stressed. Tersoff is a short range potential while AIREBO and LCBOP are long range potentials. The cutoff of Tersoff potential is 2 Å. while that of LCBOP and AIREBO is 6 and 10 Å respectively. Also there are some differences between AIREBO and LCBOP. AIREBO has a dihedral part which is not presented in LCBOP. Last but not least LCBOP has a Morse function instead of LJ. The advantage of the Morse function is that it contains more parameters so the long range part can fit better different properties in systems like graphite.

However, as we will see, is not clear where these differences are important or not in the DB problem. For instance, since in our case MD simulations were carried out (for simplicity shake) in 2D, the dihedral part in AIREBO is neglected. Also the LJ part is known to be very small compared to the strong C-C covalent bonds between nearest neighbors.

II. RESULTS

In this chapter the simulations and results will be discussed.

First of all we have checked the implementation of the different potentials in our code. It has to be noted that there is a big number of different Tersoff potentials for C, Here, the new Tersoff [31], will be used along all this work. This new potential has been optimized for graphene simulations.
Different samples have been created (a hexagonal lattice as described previously) with different lattice parameters for both BN and graphene. Our simulation cells had 576 atoms.

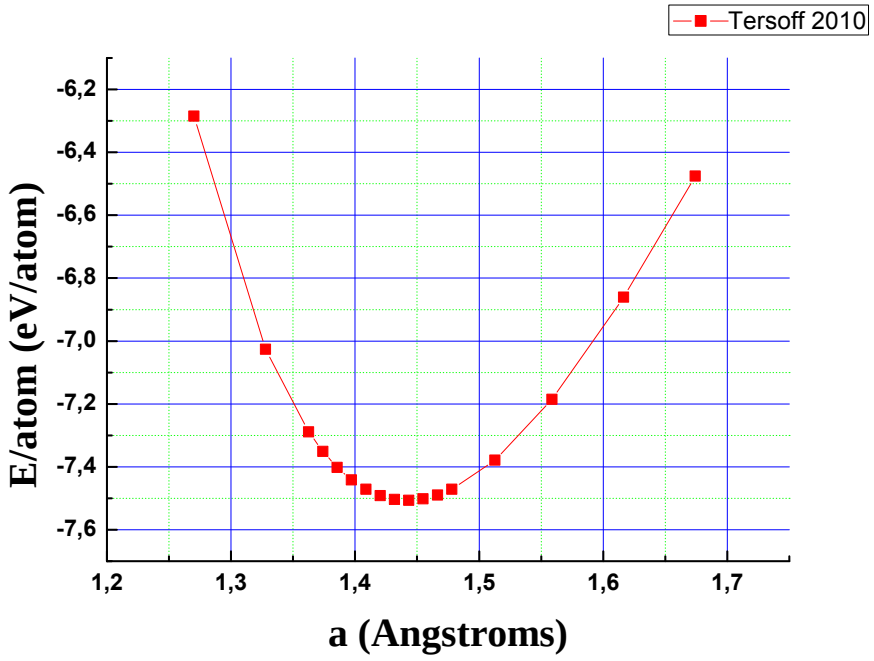

Figure 4: Energy per atom *vs* lattice constant (in Å) for 2D BN using Tersoff potential.

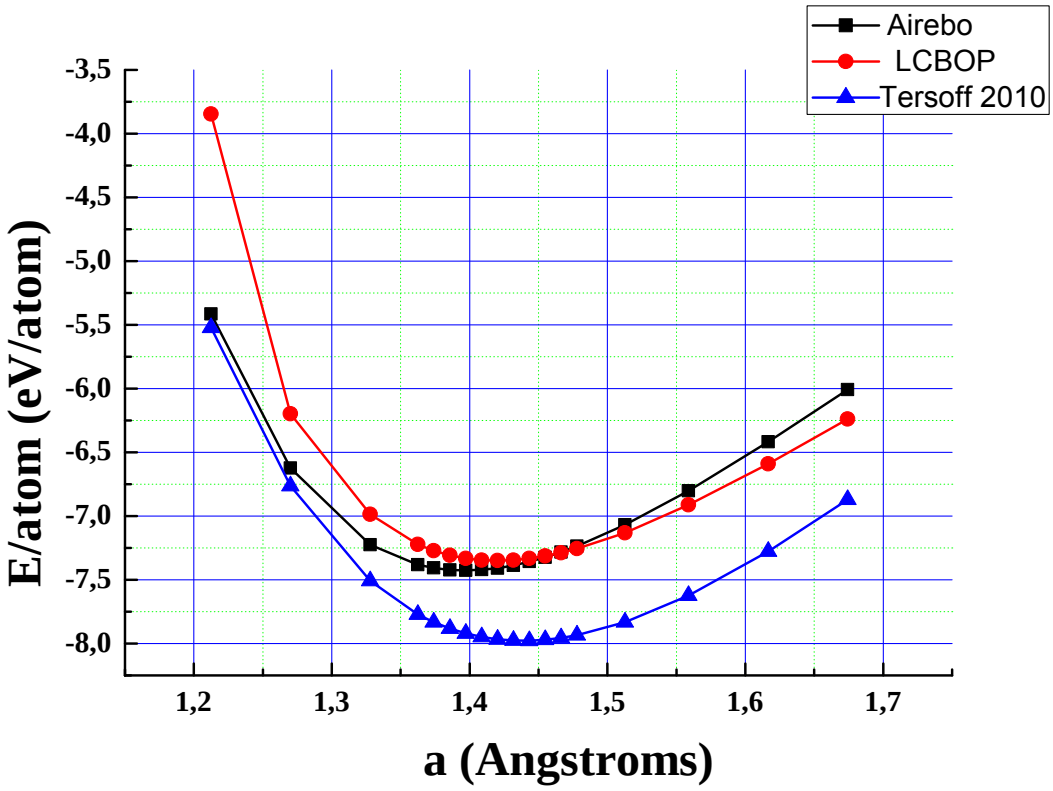

Figure 5: Energy per atom *vs* lattice constant (in Å) for 2D GE using three different potentials, AIREBO (black squares), LCBOP (red circles) and Tersoff (blue triangles) respectively.

Next table (Table 2) summarizes the results for BN and GE obtained after analyzing Figures 4 and 5.

Table 2: Shows the main results from Figures 4 and 5: cohesive energy, E_c , (eV/atom) and lattice constant a (Å) for BN and GE (with three different potentials).

	E_c (eV/atom)	a (Å)
Tersoff BN	-7,51	1,44
Experiment	-7.5[9]	1.44 [29,30]
Tersoff GE	-7,98	1,44
AIREBO GE	-7,43	1,40
LCBOP GE	-7,35	1,42
Experiment	-7.37[28]	1.42[28]

Also we have checked pressure (in Mbar) *vs* lattice constant (in Å) for 2D BN using Tersoff potential (Figure 6) and GE using AIREBO, LCBOP and Tersoff potential (Figure 7).

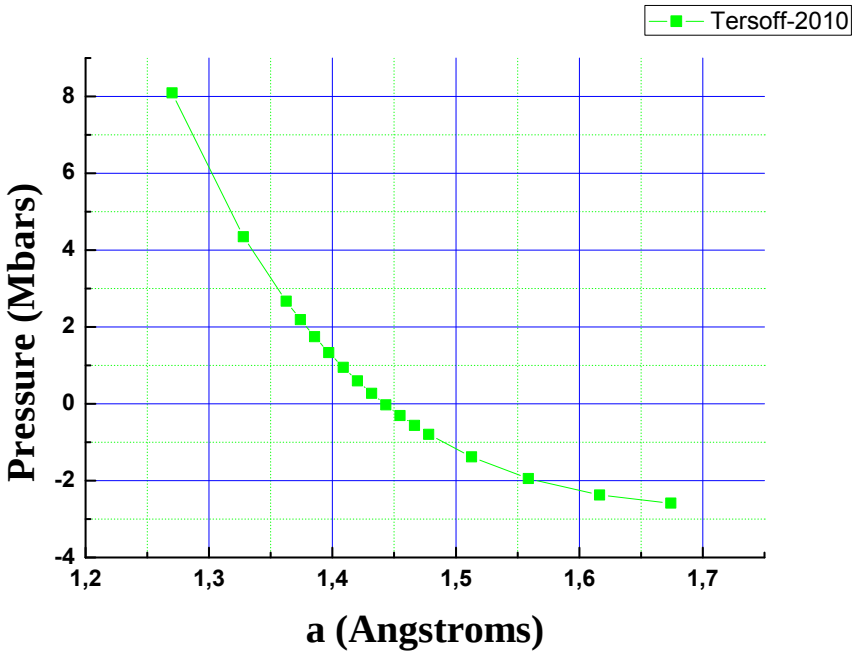

Figure 6: Pressure (in Mbar) *vs* lattice constant (in Å) for 2D BN using Tersoff potential.

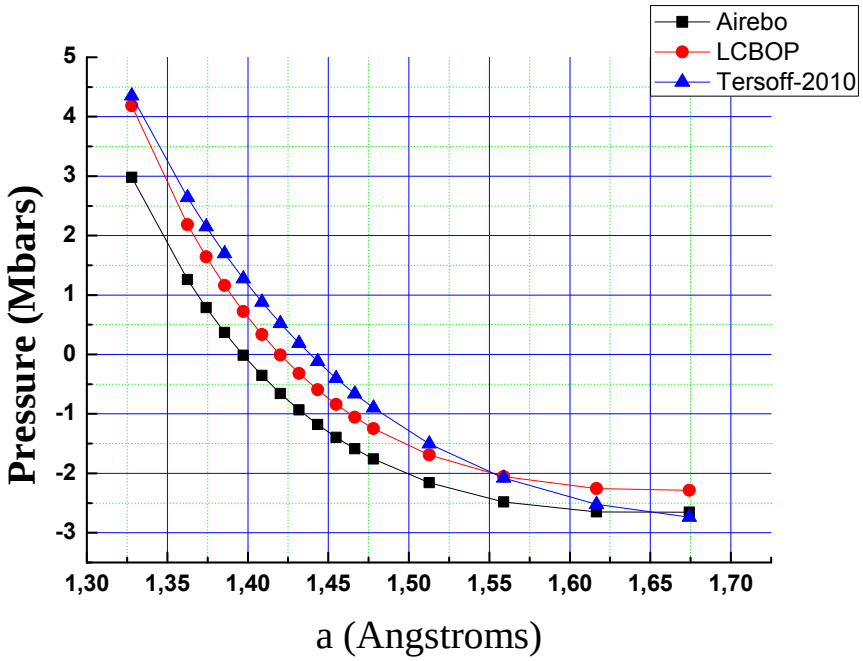

Figure 7: Pressure (in Mbar) *vs* lattice constant (in Å) for 2D GE using three different potentials, AIREBO (black squares), LCBOP (red circles) and Tersoff (blue triangles) respectively

Looking at the figures 6 and 7 we can see how pressure changes from positive to negative values around the value for the lattice parameter that correspond to the equilibrium one.

Now that samples and the potential implementation has been checked in our codes we can move to the discrete breather problem.

As explained before it is possible to create a DB moving certain atoms in a particular way [18]. That way the DB is excited and the time evolution can be followed. The following figure shows the creation of a breather using Tersoff potential. Six atoms were moved three up and three down, (See Fig. 3) with initial displacement 0.2 Å. The image was generated using OVITO [27].

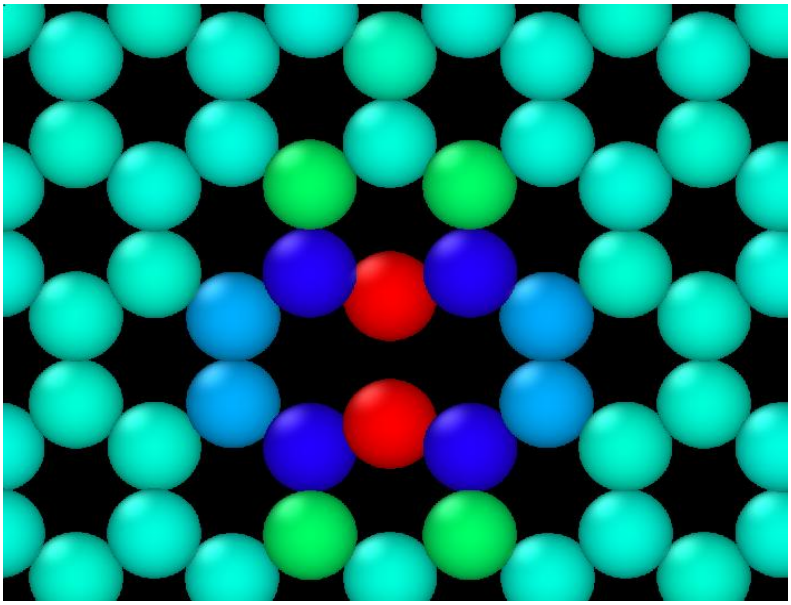

Figure 8: Breather simulation using Tersoff potential with initial displacement of six atoms equal to 0.2 Å.

Figure 8 shows the energy landscape of a DB. The two red and four dark blue atoms are the atoms initially displaced. The structure seems to be stable for a fairly long time ($\tau > 10$ ps)

The next example (Figure 9) presents the time evolution of a DB simulation. Here the simulation was carried out using LCBOP potential, the initial displacement equal to 0.2 Å and the simulation cell contains ~5000 atoms.

As before the color correspond to the energy scale. Some energy seems still localized after 2 ps, however the difference of the atoms in the hot spot (green-yellow) is not very high (is less than 10%) compared to the atoms around (blue) so does not correspond to our definition of DB.

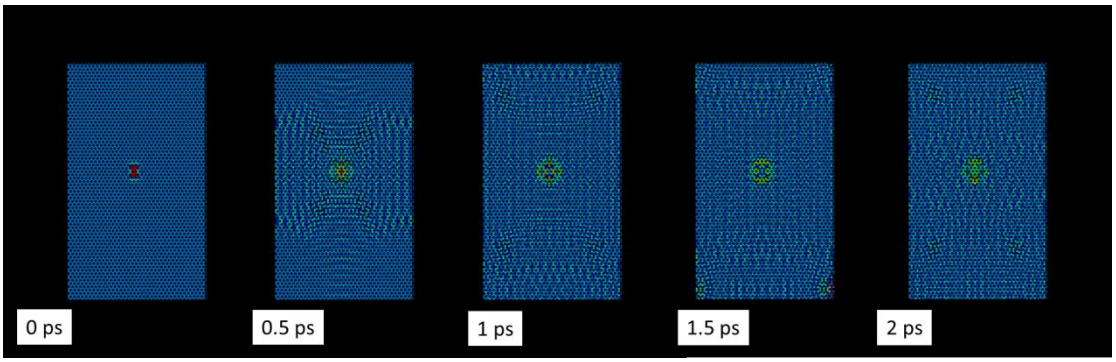

Figure 9: Sequence of a breather simulation with LCBOP potential (NVE, 0 K). Initial displacement 0.2 Å, Number of atoms 5000.

When MD simulations are carried out using AIREBO that aspect of the energy evolution with time is similar. Also the results depend on the initial displacement which is understandable.

Clear differences are found using different potentials. However is not so easy to understand the reason of those differences, for example the dependence with the cutoff or long range part of the potential.

To gain some insight of these differences we run some simulations moving only one atom in different directions (-y, +y, +x, +z) using different potentials as shown in next figure.

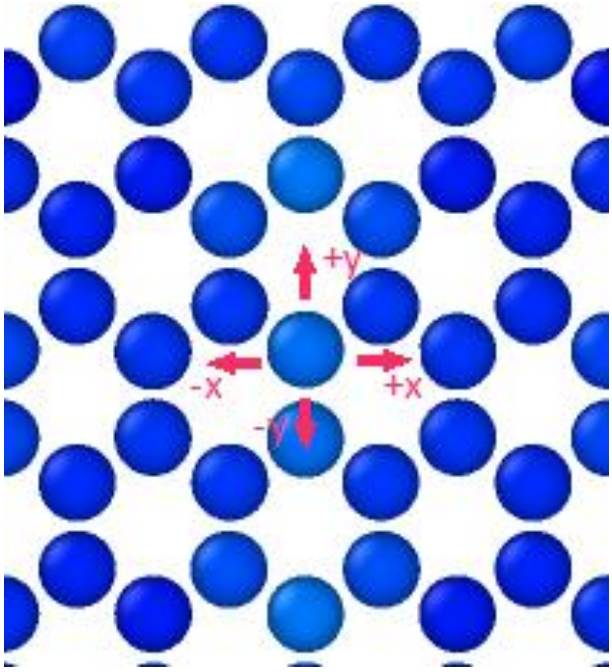

Figure 10: The different directions of the movement.

Is clear from the previous figure that in our system –y and +y are two different movements, one approaching one C atom to another one, and the other moving it far away. Moving one atom in the +x direction is equivalent to do it in the –x for obvious symmetry reasons and the same occurs for +z and –z.

Our simulation cell had 576 atoms and periodic boundary conditions are applied. Simulations are carried out in the microcanonical (NVE) ensemble, so NVE integration is used to update position and velocity for atoms in the group each timestep. The timestep, Δt, is 0.00001 ps. Also the numbers for the energy in the following graphs are only for the atom that we move. The initial displacement, d, is here 0.1 Å.

Next figure shows the results for AIREBO MD simulations. As can be seen except for the displacement out of plane (+z), the energy decay of the displaced atom in the directions +x, -y and +y is very similar.

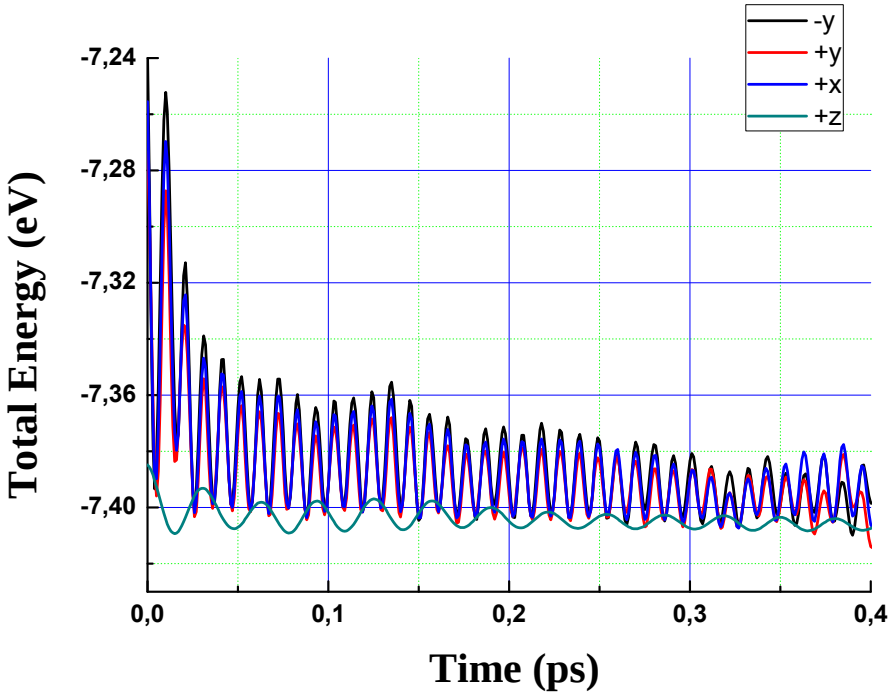

Figure 11: Energy of the displaced atom *vs* time (in ps) for 2D GE using AIREBO potential for the movement in four different directions, -y (black line), +y (red line), +x (blue line) and +z (green line). d = 0. 1Å.

Next figure shows the results for LCBOP. Again can be seen that except for the displacement out of plane, the energy decays after the displacement in the directions +x, -y and +y are similar. However here there is something different. Now the energy oscillations remain for longer times and the amplitude remains constant for longer times.

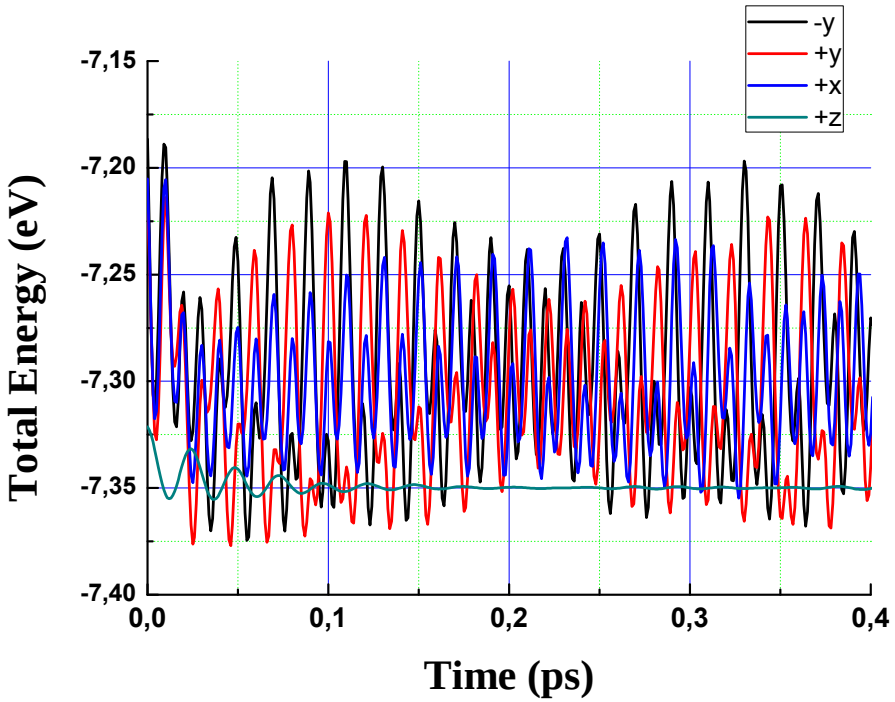

Figure 12: Energy of the displaced atom *vs* time (in ps) for 2D GE using LCBOP potential for the movement in four different directions, -y (black line), +y (red line), +x (blue line) and +z (green line). d = 0. 1Å.

Figure 13 shows the results for Tersoff. The energy decay is here similar to that observed using AIREBO (See Figure 11). The energy decays after the displacement in the directions +x, -y and +y are similar.

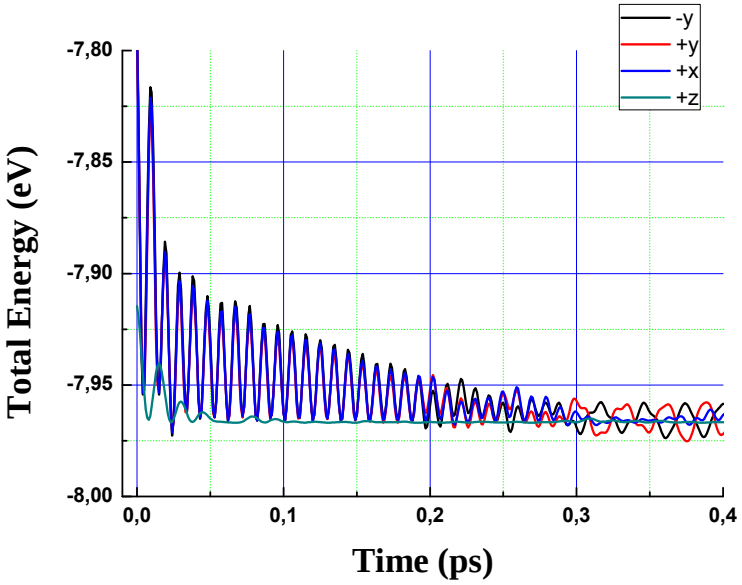

Figure 13: Energy of the displaced atom *vs* time (in ps) for 2D GE using Tersoff potential for the movement in four different directions, -y (black line), +y (red line), +x (blue line) and +z (green line). d = 0. 1Å.

Let us focus here in the very first steps of the simulation, up to 0.35 ps (See figure 14, 15 and 16). That way we can observe the differences for the different movements (or different direction) with the different potentials (see Table 3). Next figure shows the energy of the displaced atom as a function of time for 2D GE using AIREBO potential. As can be seen the differences are almost negligible (except regarding the +z displacement).

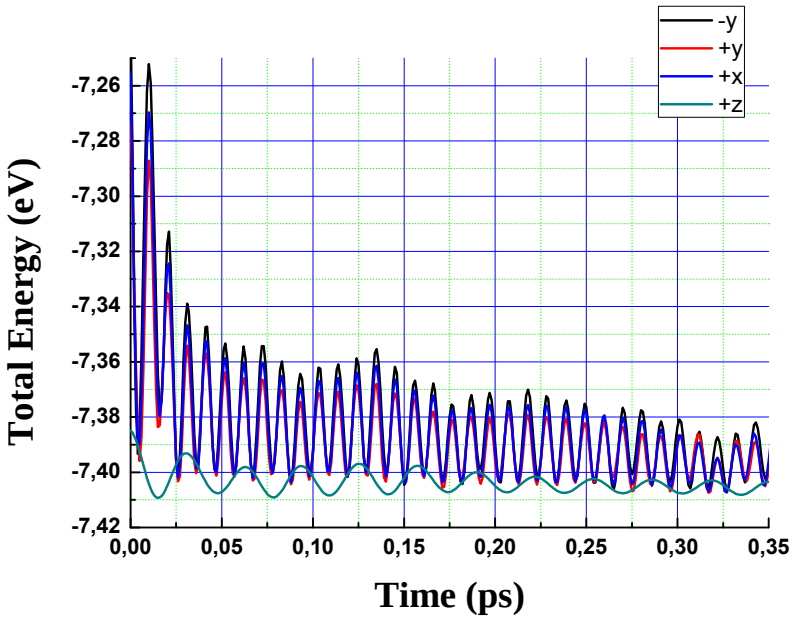

Figure 14: Energy of the displaced atom *vs* time (in ps) for 2D GE using AIREBO potential for the movement in four different directions, -y (black line), +y (red line), +x (blue line) and +z (green line). d = 0. 1Å.

Figure 15 shows now the energy of the displaced atom as a function of time using the LCBOP potential. Here the oscillations in the energy decay are slightly different depending on the direction of the displacement. What is more important, these oscillations, even if the amplitude is small, remain for longer times compared to the same ones observed with other potentials.

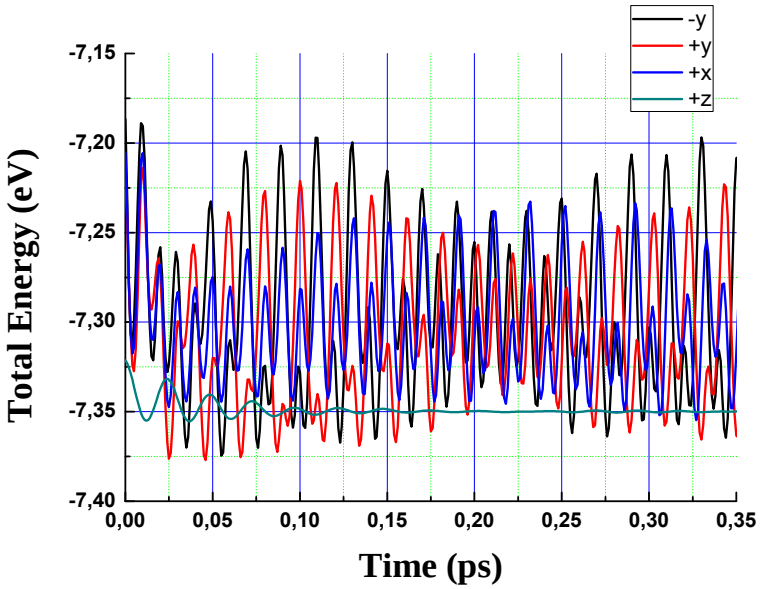

Figure 15: Energy of the displaced atom *vs* time (in ps) for 2D GE using LCBOP potential for the movement in four different directions, -y (black line), +y (red line), +x (blue line) and +z (green line). d = 0. 1Å.

Finally Figure 16 shows the same results as before now using Tersoff potential. As observed when using AIREBO (Fig 14) here, the oscillations in the energy decay are almost identical independently of the direction of the displacement.

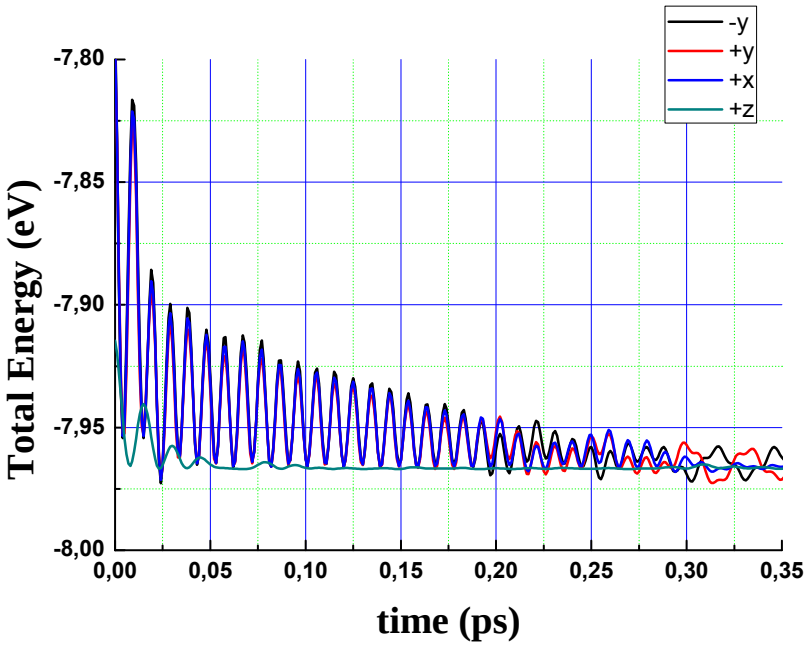

Figure 16: Energy of the displaced atom *vs* time (in ps) for 2D GE using Tersoff potential for the movement in four different directions, -y (black line), +y (red line), +x (blue line) and +z (green line). d = 0. 1Å.

The DB lifetime is usually defined as the time necessary for the DB atoms to come back to 10 % the value of the difference with respect to the surrounding atoms. In the following table the energy decay time after an atom displacement is given. As can be seen is very small in all cases except in the case of LCBOP, but in that case the energy oscillations are very small, so we do not consider it to be a DB.

Table 3: The energy decay time (ps) for the displaced atom moved in the directions -y, +y, +x, +z with the use of different potentials (AIREBO, LCBOP, Tersoff).

DIRECTION	AIREBO Lifetime (ps)	LCBOP Lifetime (ps)	TERSOFF Lifetime (ps)
-y	0.18	> 1	0.15
+ y	0.18	> 1	0.15
+ x	0.18	> 1	0.15
+ z	0.20	0.05	0.03

Also for graphene differences were observed between the energy decay after a specific movement (here 0.1 Å) with the use of different potentials as shown in next graphs.

In order to compare properly the different results we subtract the initial energy of the displaced atom, E_0, so we can better analyze the decay of the displaced atom.

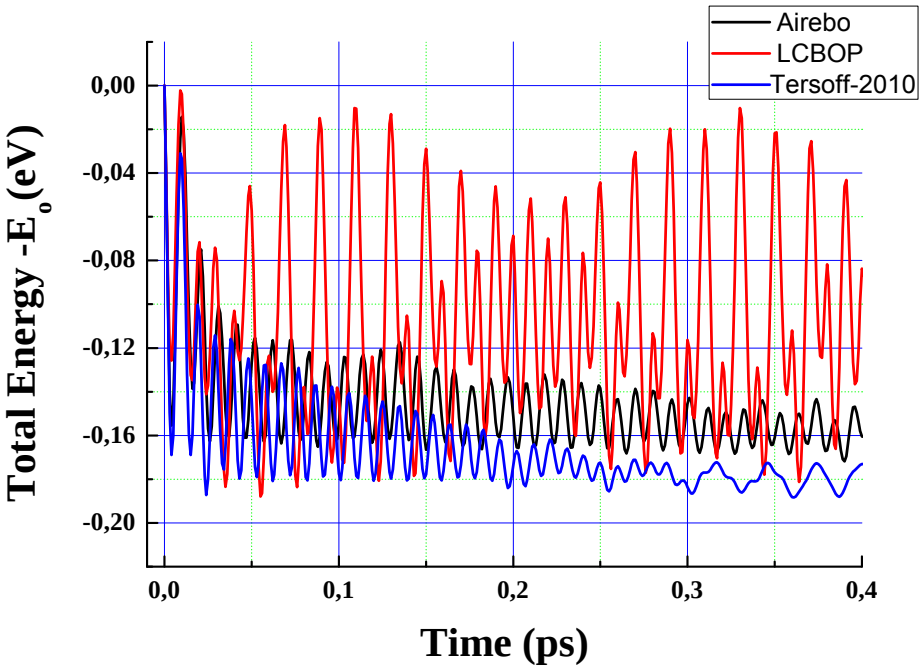

Figure 17: Energy of the displaced atom minus E_o *vs* time (in ps) for 2D GE using three different potentials, AIREBO (black line), LCBOP (red line) and Tersoff (blue line) for the movement in directions –y.

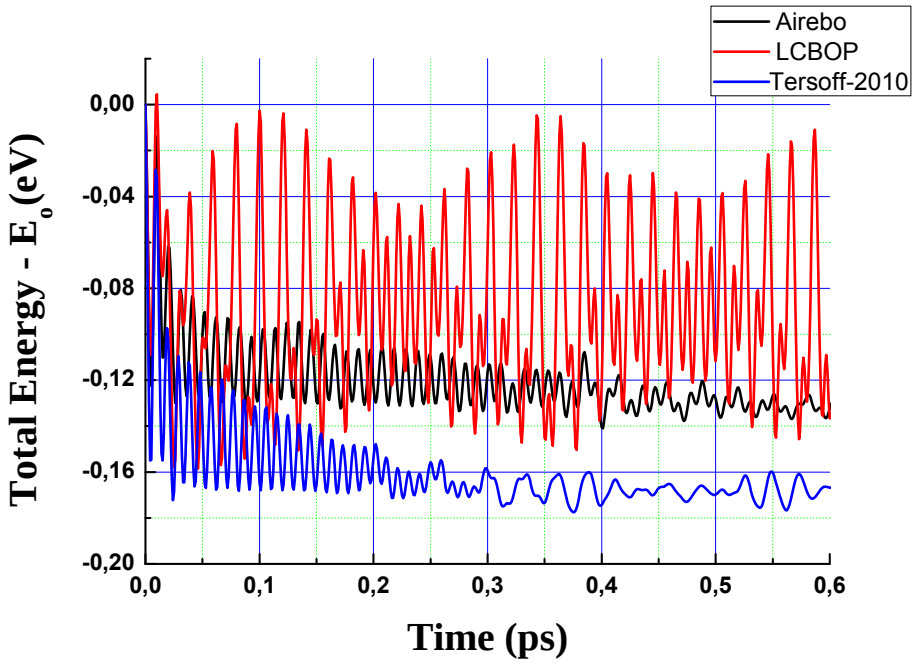

Figure 18: Energy of the displaced atom minus E_o *vs* time (in ps) for 2D GE using three different potentials, AIREBO (black line), LCBOP (red line) and Tersoff (blue line) for the movement in directions +y.

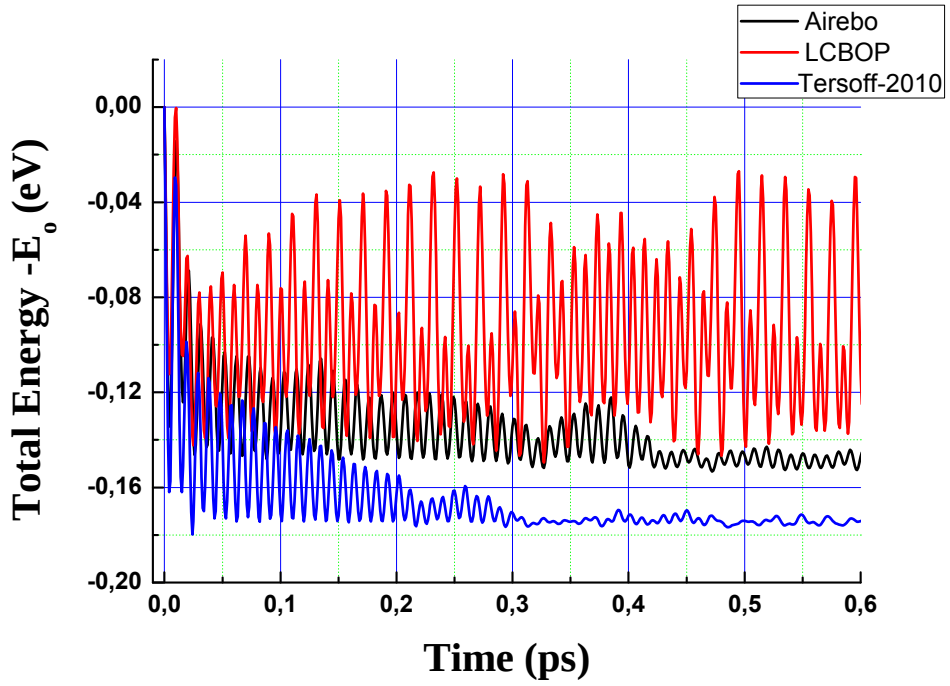

Figure 19: Energy of the displaced atom minus E_o *vs* time (in ps) for 2D GE using three different potentials, AIREBO (black line), LCBOP (red line) and Tersoff (blue line) for the movement in directions +x.

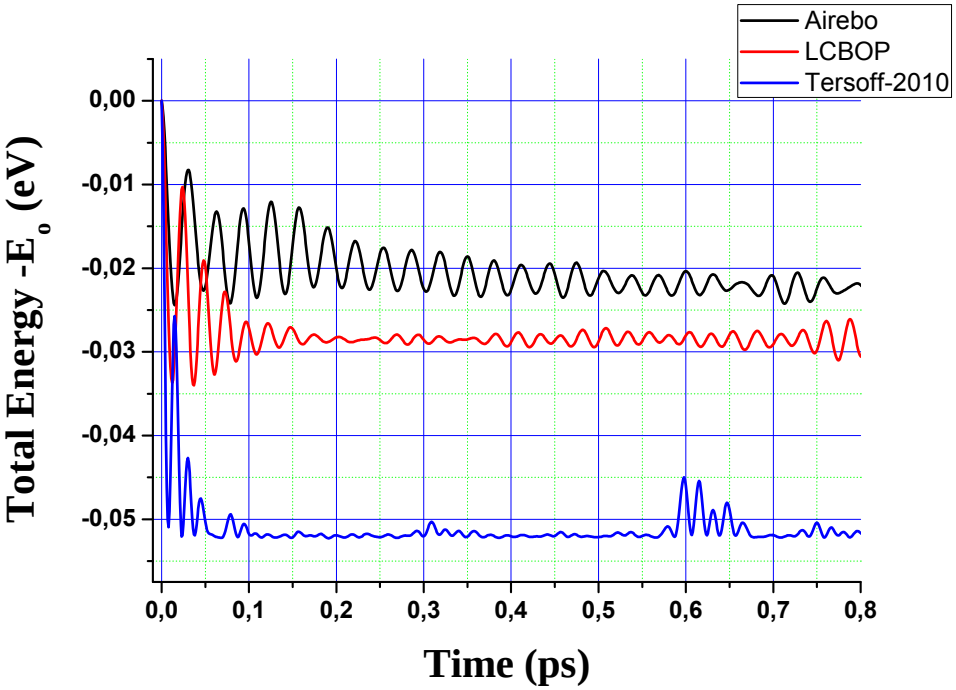

Figure 20: Energy of the displaced atom minus E_o *vs* time (in ps) for 2D GE using three different potentials, AIREBO (black line), LCBOP (red line) and Tersoff (blue line) for the movement in directions +z.

Now the difference between the energy decay after a different displacement using the LCBOP potential are shown in next graphs.

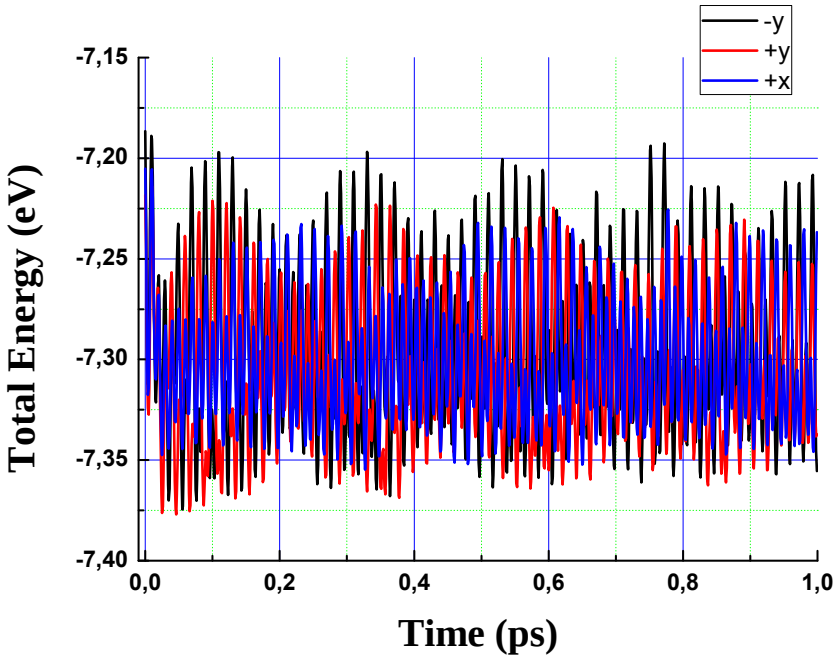

Figure 21: Total energy of the displaced atom *vs* time (in ps) for 2D GE using LCBOP potential for the movement in three different directions, -y (black line), +y (red line) and +x (blue line) with initial distance 0.1 Å.

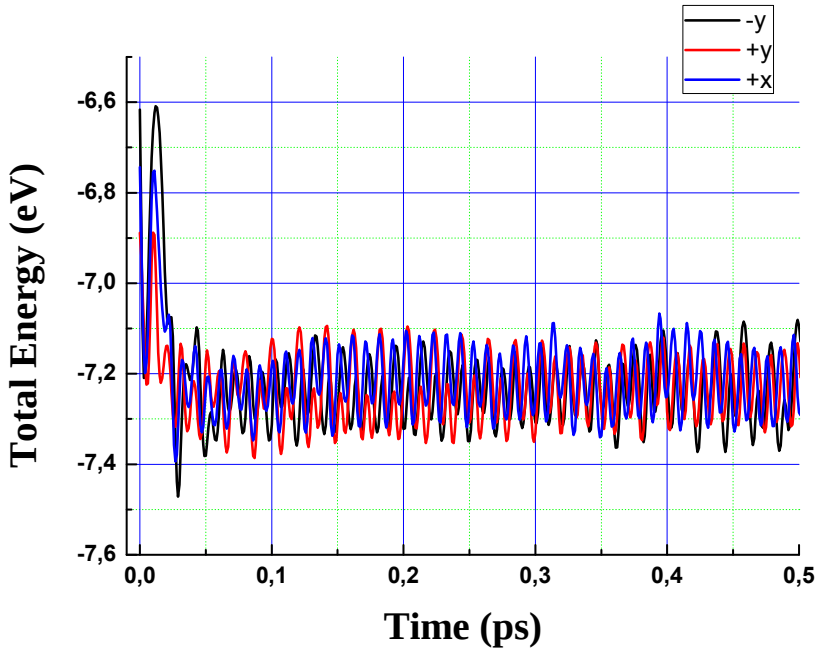

Figure 22: Energy of the displaced atom *vs* time (in ps) for 2D GE using LCBOP potential for the movement in three different directions, -y (black line), +y (red line) and +x (blue line) with initial distance 0.2 Å.

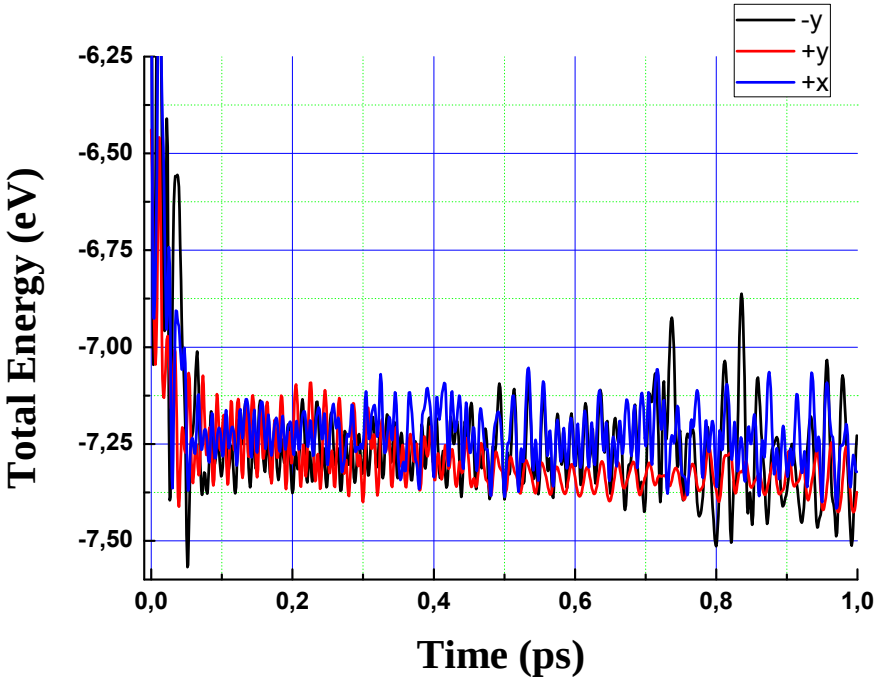

Figure 23: Energy of the displaced atom *vs* time (in ps) for 2D GE using LCBOP potential for the movement in three different directions, -y (black line), +y (red line) and +x (blue line) with initial distance 0.3Å.

As can be seen in the previous graphs the amplitude of the energy oscillations increases with the initial displacement, ranging from 0.15 eV to 0.3 eV when d changes from 0.1 to 0.3 Å. However, the amplitude of these energy oscillations after a displacement of 0.3 Å is more chaotic (the value is not constant with time) in all cases, i.e. after a displacement on ±y or x.

Apart of the energy relaxation and the oscillations of this decay is obvious that the energy jump, ΔE, after the displacement will depend in the value of the displacement. In the following table the energy jump is given for the different directions. First thing to be noticed here is that the value of ΔE is almost direction independent.

Table 4: Energy jump for the different directions of the displacement using AIREBO interatomic potential.

AIREBO			
	ΔE (eV) (d=0,1 Å)	ΔE (eV) (d=0,2 Å)	ΔE (eV) (d=0,3 Å)
-y	0,14	0,12	0,30
+y	0,11	0,09	0,25
+x	0,10	0,07	0,22

Next table presents the ΔE values for different directions and displacements using LCBOP potential. The value of ΔE is almost direction independent (as with AIREBO) when the displacement is small but, clearly depends in this direction when the displacement is high (0.2 Å or bigger). As expected the value the bigger the displacement the bigger is ΔE.

Table 5: LCBOP was used for the computation of energy jump for different directions

LCBOP			
	ΔE (eV) (d=0.1 Å)	ΔE (eV) (d=0.2 Å)	ΔE (eV) (d=0.3 Å)
-y	0.13	0.6	1.4
+y	0.11	0.5	0.9
+x	0.11	0.3	0.5

Finally next table shows the ΔE values for different directions using Tersoff potential. The value of ΔE is almost direction independent (as with AIREBO).

Table 6: Energy jump for the different directions of the displacement with the use of Tersoff potential.

TERSOFF			
	ΔE (eV) (d=0,1 Å)	ΔE (eV) (d=0,2 Å)	ΔE (eV) (d=0,3 Å)
-y	0,14	0,11	0,25
+y	0,13	0,09	0,15
+x	0,12	0,10	0,11

Next set of graphs represent the visual inspection of the time evolution of our system after different displacements (left column). The energy scale is given in the right column for GE using Tersoff potential. The images were created using OVITO [27].

TERSOFF (d=0.1Å)				
	0ps	0.5ps	1ps	
-y	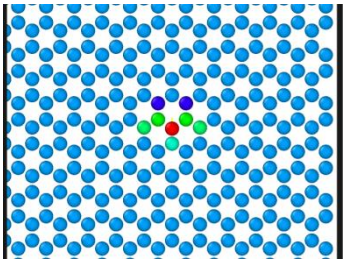	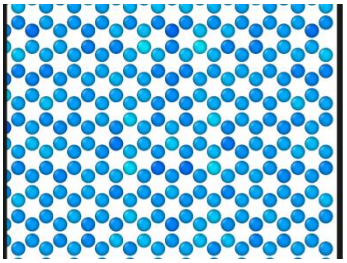	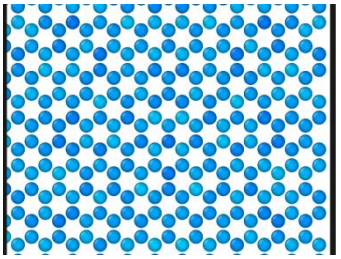	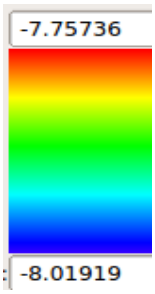
+y	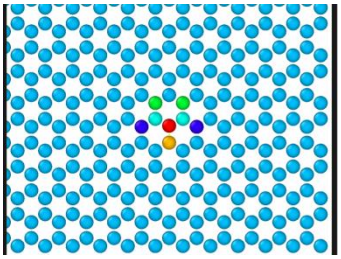	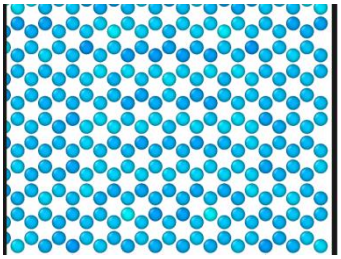	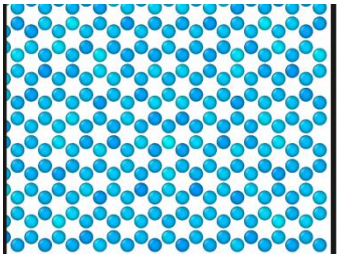	
+x	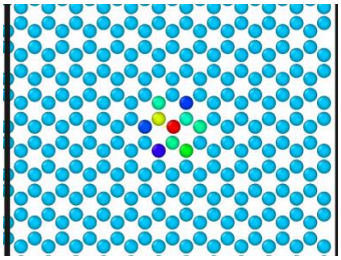	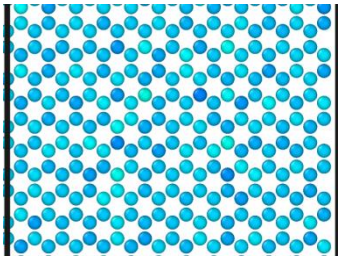	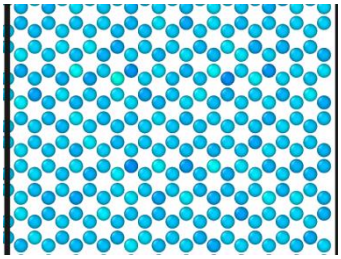	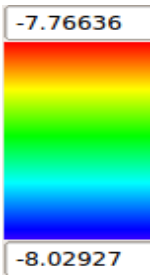
+z	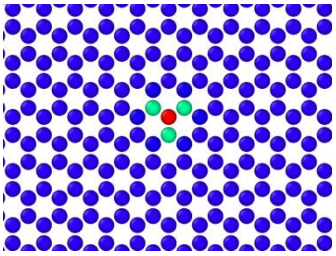	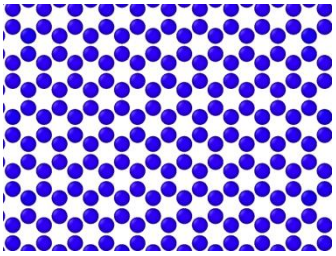	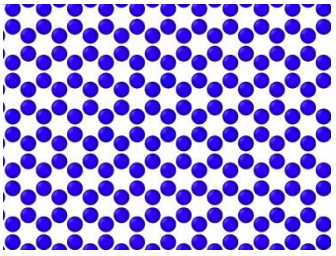	

The following set of graphs represents the visual inspection of the time evolution of our system after different displacements (left column). The energy scale is given in the right column for GE using AIREBO potential.

AIREBO (d=0.1Å)				
	0ps	0.5ps	1ps	
-y	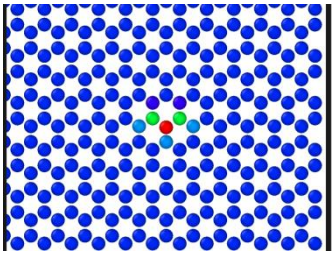	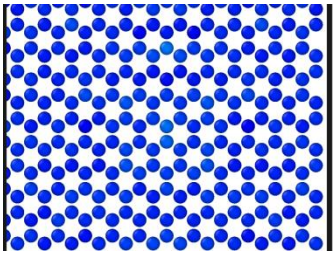	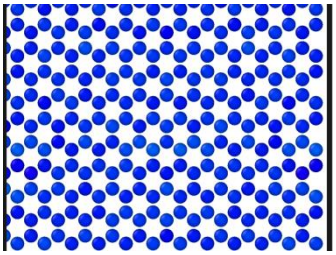	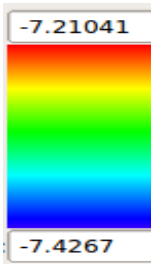
+y	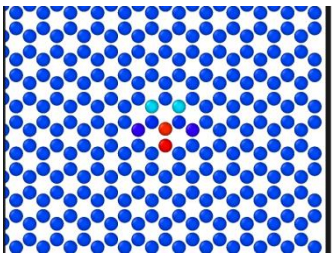	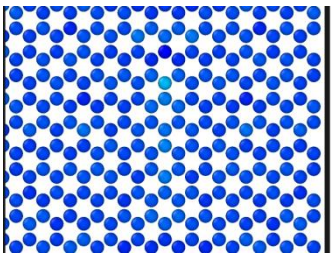	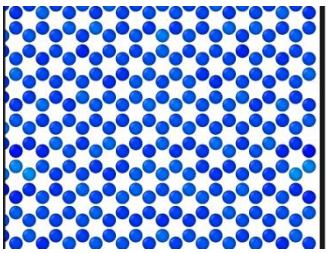	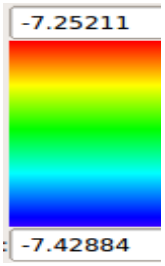
+x	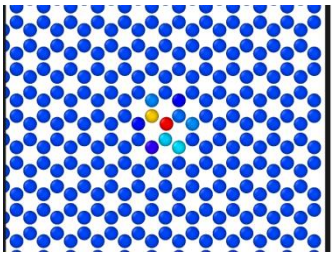	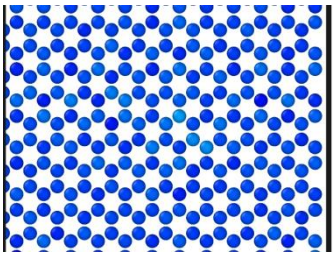	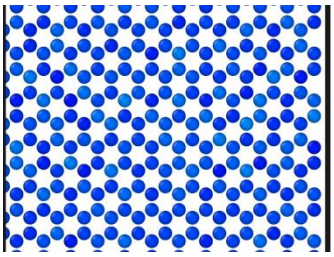	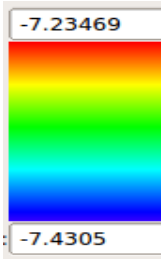
+z	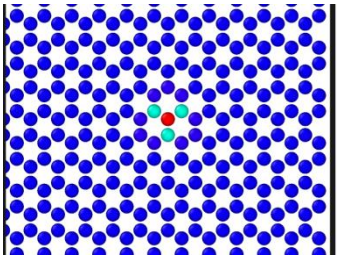	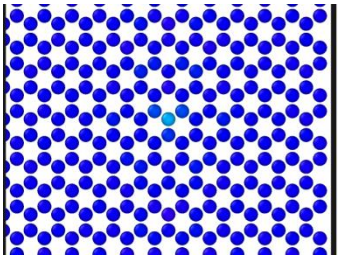	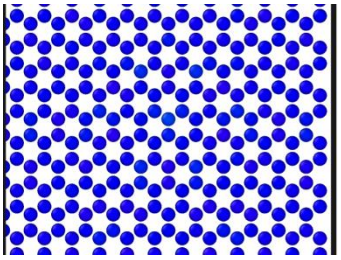	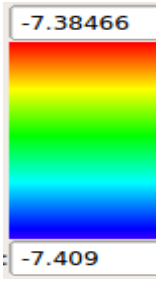

As before next set of graphs represent the time evolution of GE using LCBOP potential after different displacements (left column). The energy scale is given in the right column.

LCBOP (d=0.1Å)				
	0ps	0.5ps	1ps	
-y	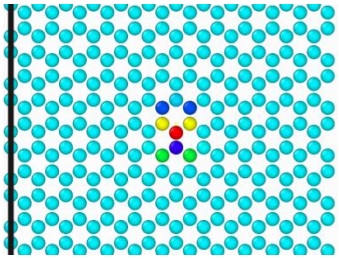	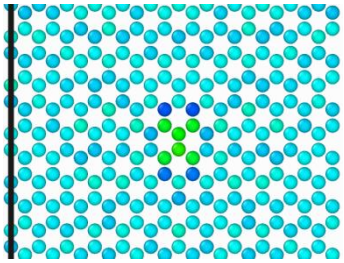	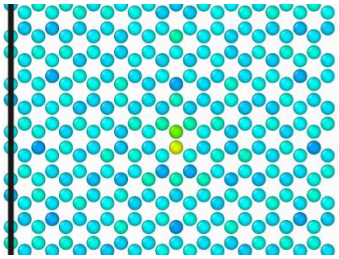	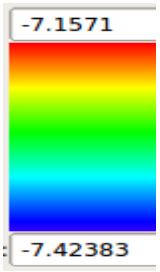
+y	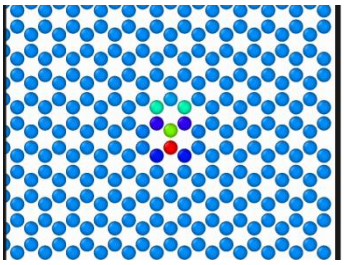	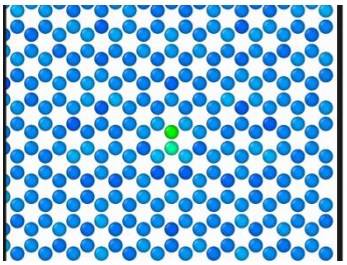	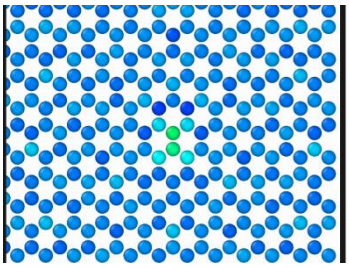	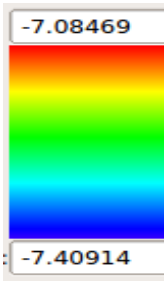
+x	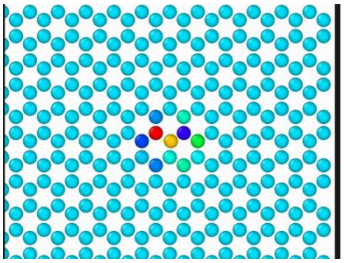	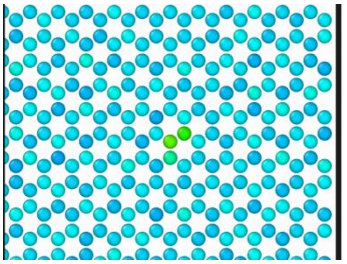	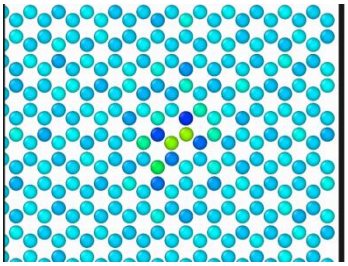	
+z	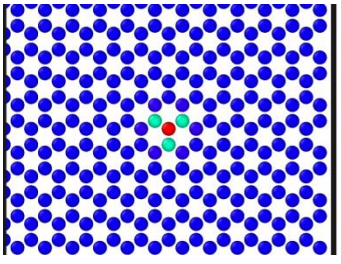	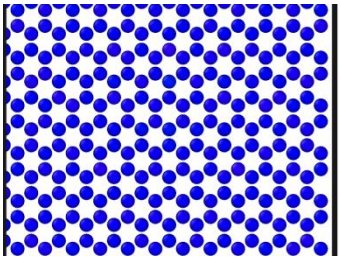	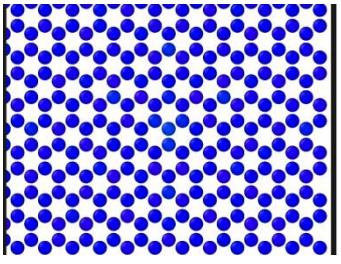	

As before, the time evolution of GE using LCBOP potential after different displacements (left column) is shown. Now the displacement is 0.2 Å. The energy scale is given in the right column.

LCBOP (d=0.2Å)				
	0 ps	0.5 ps	1ps	
-y	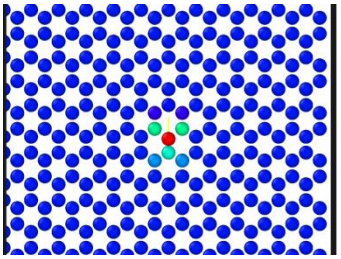	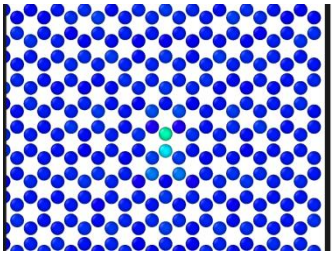	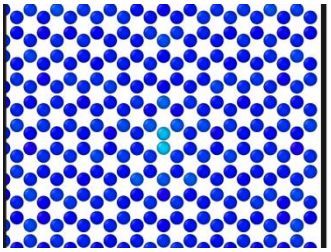	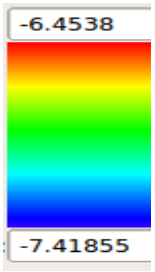
+y	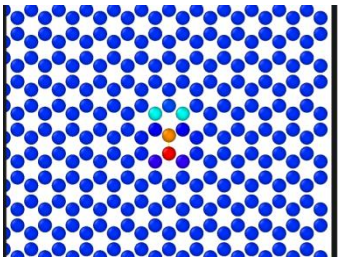	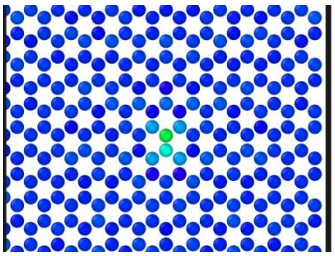	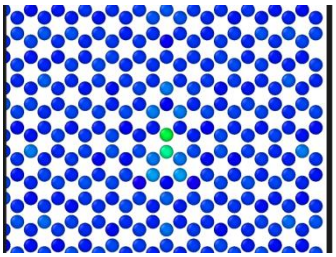	
+x	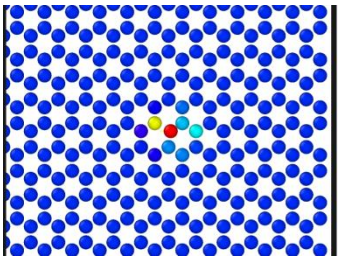	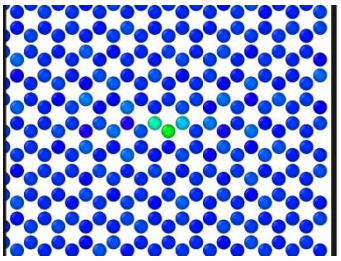	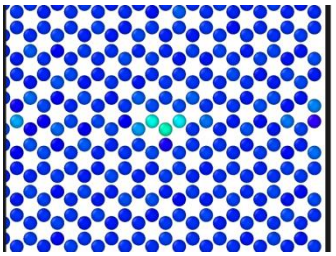	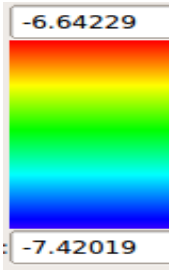

In the last set of graphs the time evolution of GE using LCBOP potential after different displacements (left column) is shown. Now the displacement is 0.3 Å. The energy scale is given in the right column.

LCBOP (d=0.3Å)				
	0 ps	0.5 ps	1 ps	
-y	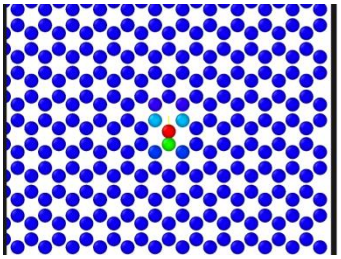	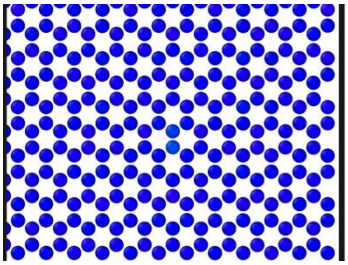	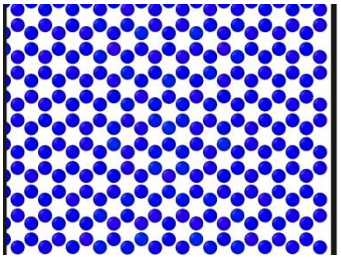	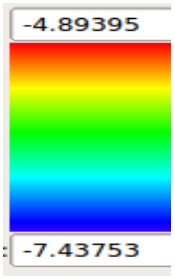
+y	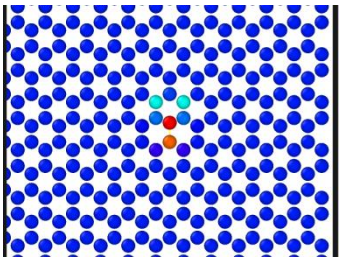	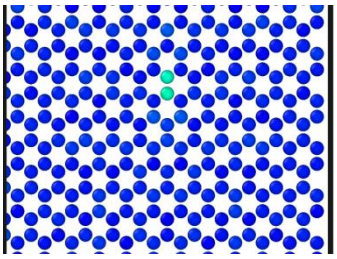	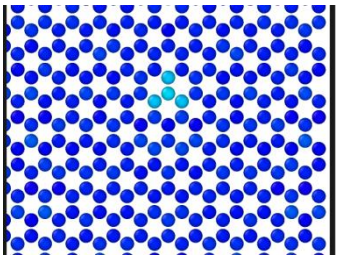	
+x	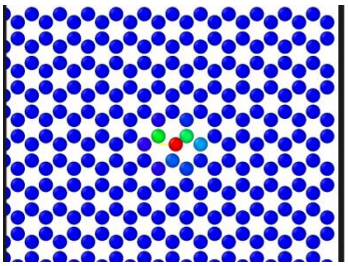	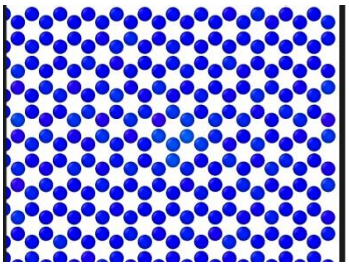	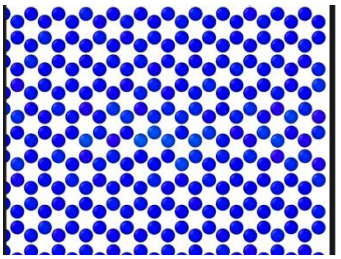	

Let us move now to the differences regarding the displacement of the atoms when using the three different potentials. Next figures show the displacement respect the original position of the displaced atom in three different cases, namely -y, +y and +x, and figures 24, 25 and 26 respectively.

As can be seen the atom displacements using AIREBO and Tersoff are very similar while the atoms seems more free to move when using the LCBOP since they oscillate for longer periods around the original position.

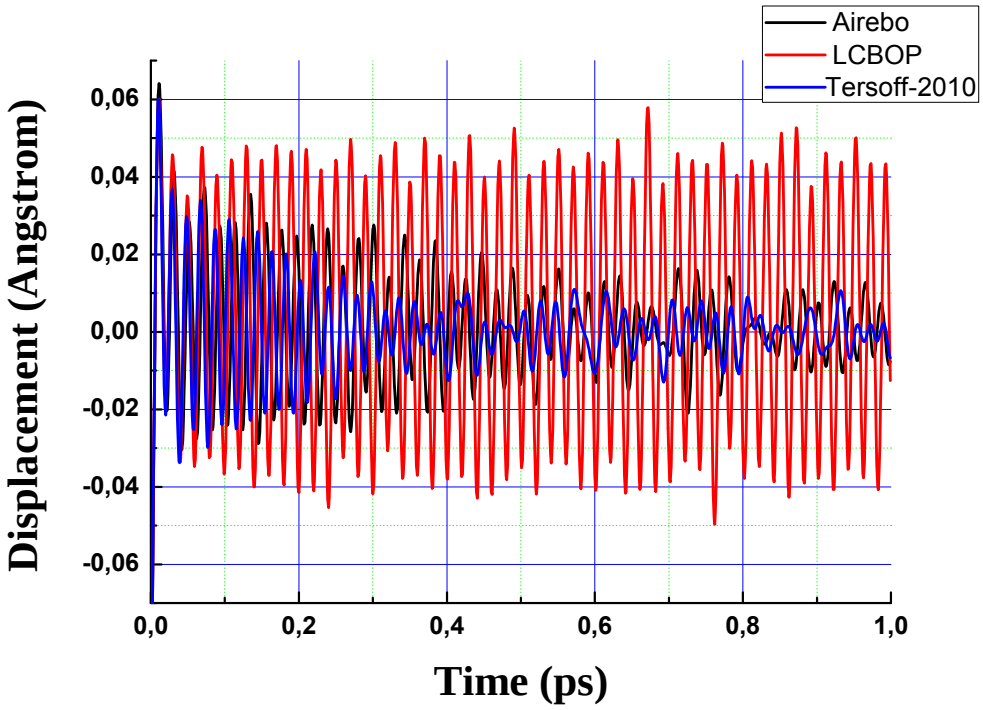

Figure 24: Displacement of the displaced atom *vs* time (in ps) for 2D GE using three potential for the movement in direction, -y with initial distance 0.1 Å.

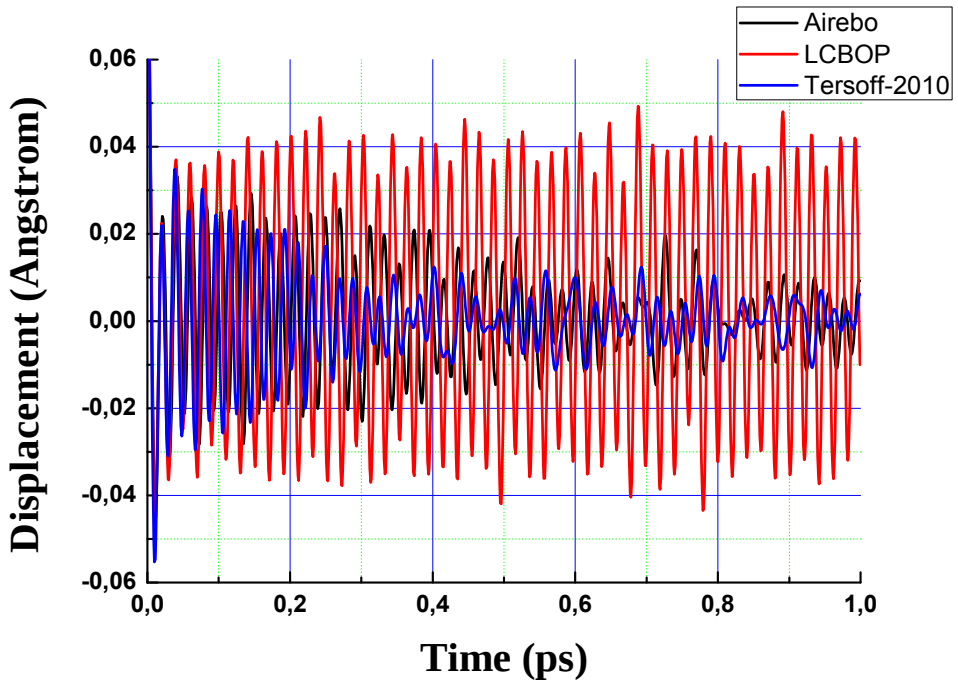

Figure 25: Displacement of the displaced atom *vs* time (in ps) for 2D GE using three different potentials, Airebo, LCBOP and Tersoff for the movement in direction +y with initial distance 0.1 Å.

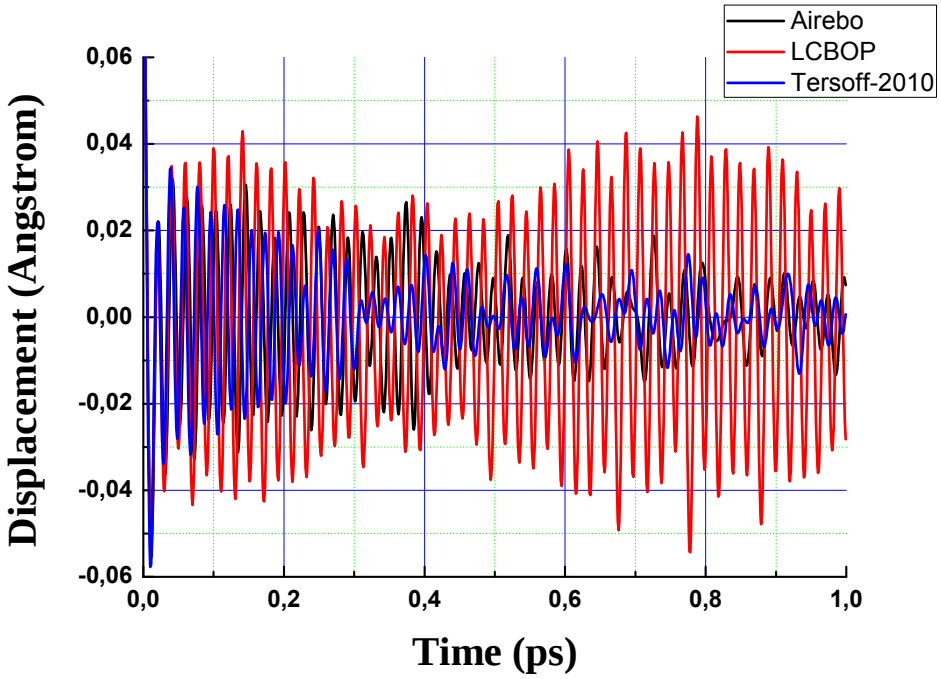

Figure 26: Displacement of the displaced atom *vs* time (in ps) for 2D GE using three different potentials, AIREBO, LCBOP and Tersoff for the movement in direction +x with initial distance 0.1 Å.

For BN we have the following graphs.

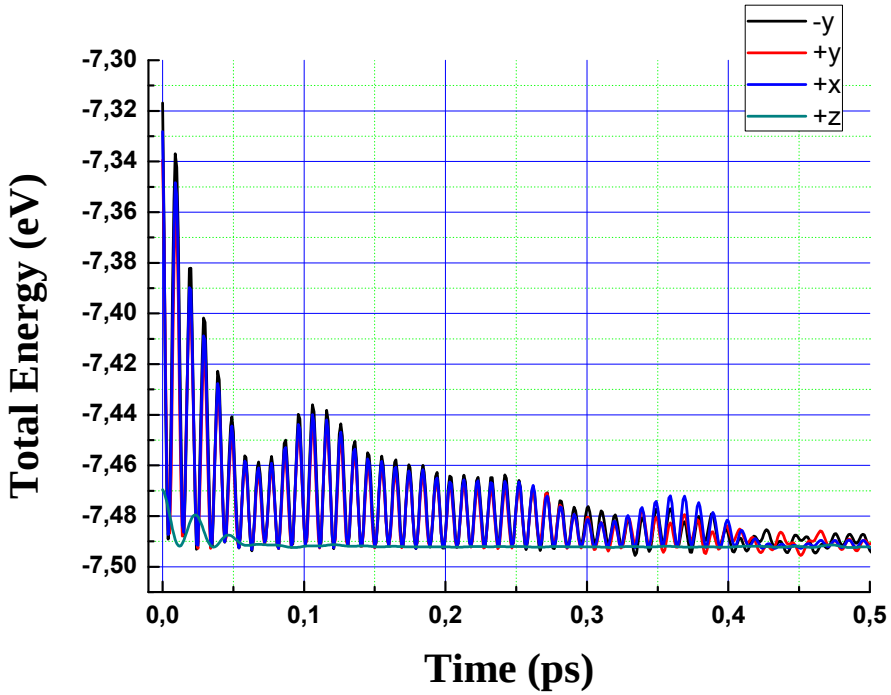

Figure 27: Energy of the displaced atom *vs* time (in ps) for 2D BN using Tersoff potential for the movement in four different directions, -y (black line), +y (red line), +x (blue line) and +z (green line).

Next figure shows the lifetime for the movement to directions +y, -y and +x and the results are sawn in the Table 7.

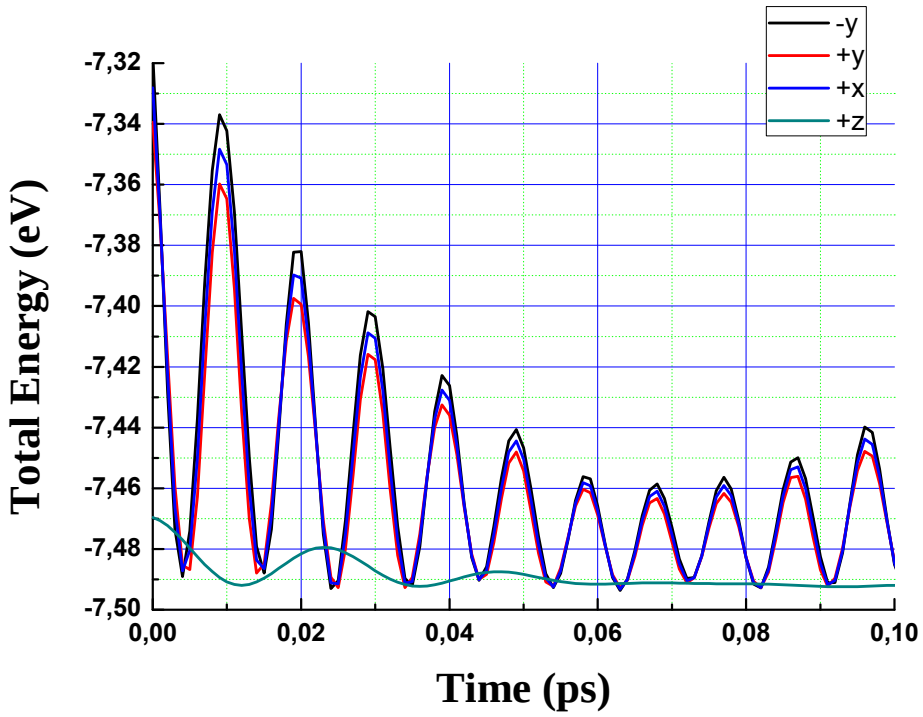

Figure 28: Energy of the displaced atom *vs* time (in ps) for 2D BN using Tersoff potential for the movement in four different directions, -y (black line), +y (red line), +x (blue line) and +z (green line)..

Table 7: Disturbance lifetime (ps) for BN after different initial displacement in directions -y, +y and +x using of Tersoff potential.

DIRECTION	TERSOFF Lifetime (ps) 0.1	TERSOFF Lifetime (ps) 0.2	TERSOFF Lifetime (ps) 0.3
-y	0.06	0.06	0.06
+ y	0.06	0.06	0.06
+ x	0.06	0.06	0.06

Next set of graphs represent the visual inspection of the time evolution of our system after different displacements (left column). The energy scale is given in the right column for BN using Tersoff potential.

	0ps	0.5ps	1ps	
-y	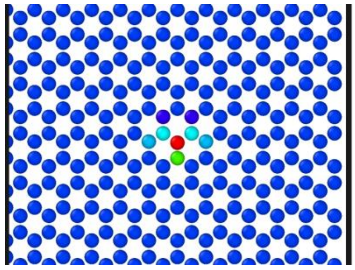	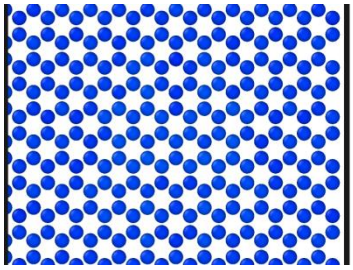	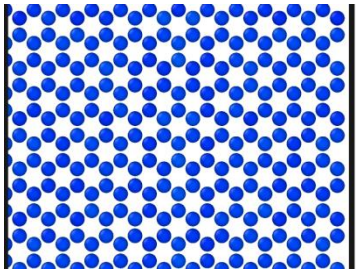	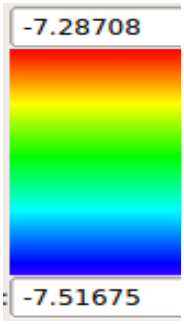
+y	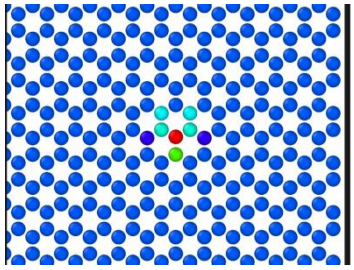	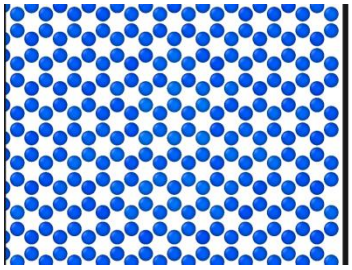	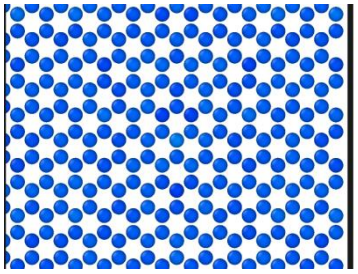	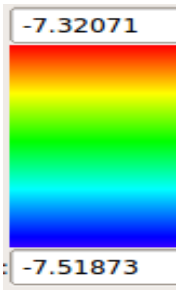
+x	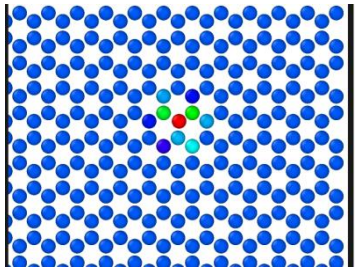	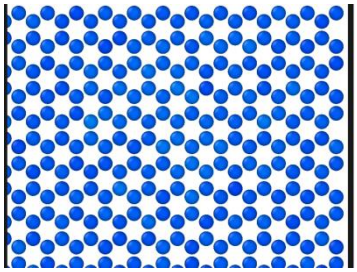	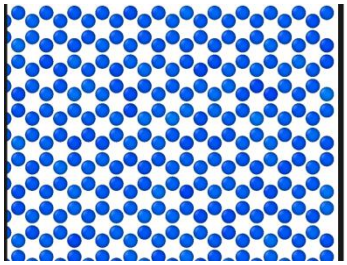	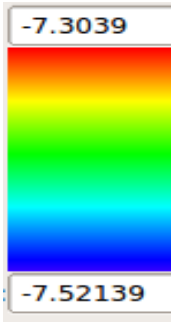
+z	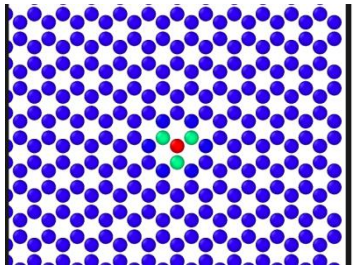	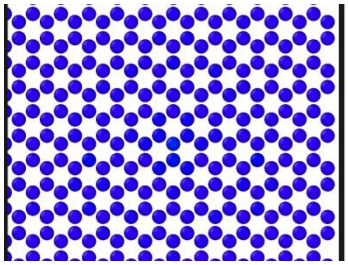	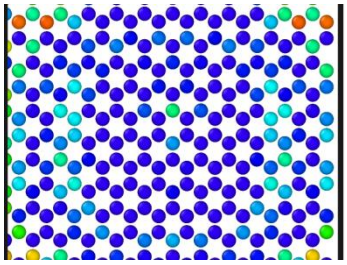	

The perturbation created after displacing one atom (B in this case) in BN disappears fast in all the investigated cases. The last example (+z) reminds the work Chechin [17] where they created the DB moving one H atom out of plane in graphane. However here we can not see any DB.

Clearly there are little differences between the different potentials regarding to the decay of the energy after the displacement of a single atom. Hence there is not much information we can obtain from that in order to understand the DBs properties depending on the potential. To conclude we have repeated the simulations moving two atoms towards each other (+y and –y, see Figure 29). Again the simulations are carried out in NVE ensemble with periodic boundary conditions.

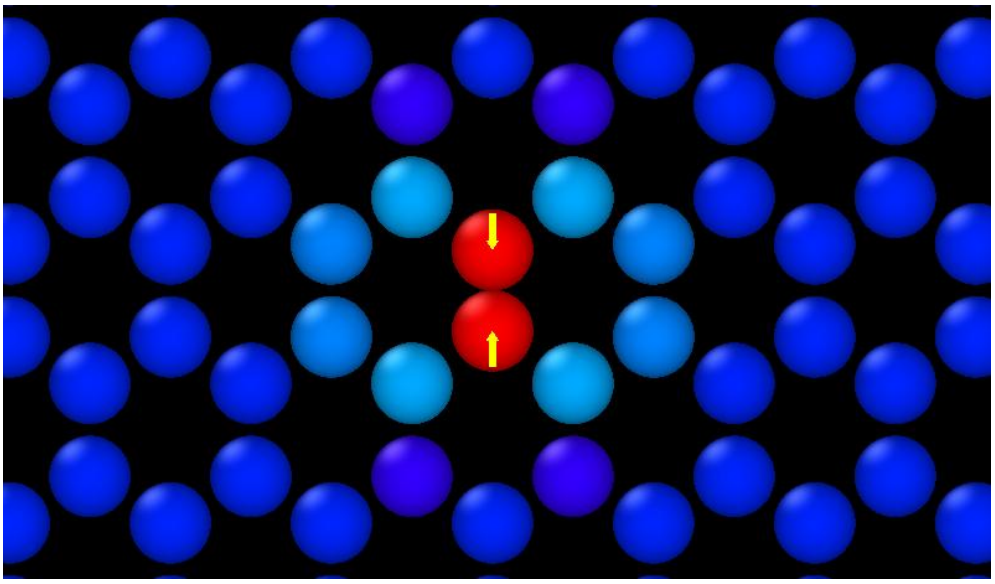

Figure 29: Schematic illustration of the initial condition to generate ILMs. (Yellow arrows are not a scale).

This way we can observe breathers with lifetimes clearly longer than 1ps. Next table summarizes the results: The values between parenthesis indicates the estimated lifetime, τ, in ps. For AIREBO an initial displacement of 0.3 Å is too big and melting starts.

Table 8: Disturbance lifetime (ps) for GE and BN after different initial displacement using different potentials.

Potentials	d (Å)				
	0,1	0,15	0,2	0,25	0,3
TERSOFF GE	No	No	Yes (>1)	Yes (>1)	Yes (>10)
AIREBO	No	Yes (>1)	No	Yes (>1)	Melting
LCBOP	No	No	No	No	No
TERSOFF BN	No	No	No	No	No

It has to be noted that moving 6 atoms in the way shown in Figure 3 the DBs created with AIREBO or LCBOP (See Figure 9) were not stable, while now, just moving two atoms it is possible indeed to observe fairly stable DBs with AIREBO.

AIREBO (d=0.15Å)			
0ps	0.1ps	1ps	
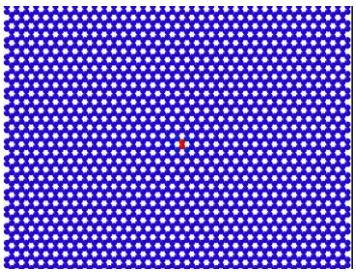	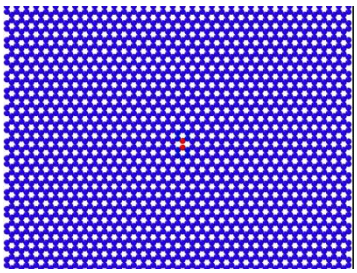	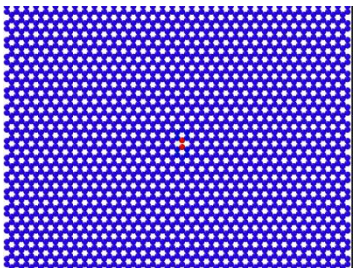	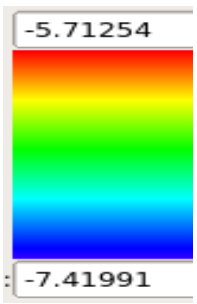

III. CONCLUSIONS

We have investigated the differences in the relaxation process using different potentials. Just moving one atom these differences are small. The results using AIREBO and Tersoff are similar while LCBOP presents different features. The decay of the energy is faster in AIREBO and Tersoff, while with LCBOP the oscillations remains for longer times. However this oscillations are small in amplitude (±0.1 eV).
The frequency of those oscillations is almost the same with all the three potentials, around 80 THz.

We have found that moving two atoms (one towards the other) it is possible indeed to create a DB. For Tersoff potential there is a threshold in the displacement around 0.2 Å, and then, if the displacement is 0.2 Å or bigger the DB is stable (this corresponds to ΔE of value 0.18eV).

Interestingly, something more complex is found for AIREBO. In this case the DB can be found with a displacement of only 0.15 Å (ΔE=0.19eV) and then, if the displacement is 0.2 Å the DB is not stable, but again, moving the atom a displacement of 0.25 Å (ΔE=0.28 eV) the DB is created and is stable for at least 1 ps.

Interestingly with LCBOP the oscillations of the energy after moving one atom seems to be more stable and hence a DB formation seemed easier.

Also there is some important difference between LCBOP and AIREBO and Tersoff. In the first one is clear than the atoms are somewhere less bonded to the neighbors since they oscillate freely during longer times.

However, moving two atoms we found DBs (depending on the displacement) in both AIREBO and Tersoff, but never with LCBOP.
Interestingly, moving 6 atoms in the way shown in Figure 3 the DBs created with AIREBO or LCBOP were not stable, while just moving two atoms it was possible to observe very stable DBs, but only with AIREBO, not with LCBOP.

For BN we can not compare different potentials. Hence only the comparison of the behavior of a displaced atom is possible. In short what is observed is that the energy decay is almost the same in all the in-plane directions.

More important, in BN the energy added after the initial displacement disappears fast in all the investigated cases. When the atom is moved along the +z direction (out of plane) no DB is observed, in contrast to the work reported in [17], where they created DBs moving one H atom out of plane in graphane.

Is also important to note that the differences observed between AIREBO, Tersoff and LCBOP are not clear since the PhDOS is very similar with all of them.

IV. MOST USED ABREVIATIONS

2D: Two dimensions
AIREBO: Adaptive Intermolecular REBO potential
BN: Boron Nitride
DB: Discrete breather
GE: Graphene
h-BN: hexagonal Boron Nitride
ILM: Intrinsic Localized Modes
LAMMPS: Large-scale Atomic/Molecular Massively Parallel Simulator
LCBOP: Long-range Carbon Bond Order Potential
LJ: Lennard-Jones
MD: Molecular Dynamics
NVE: Constant particle Number, Volume, Energy (Microcanonical ensemble)
NVT: Constant particle Number, Volume, Temperature (Canonical ensemble)
PhDOS: Phonon Density of States
SGE: Single Graphene

V. REFERENCES

[1] A.K Geim and K.S. Novoselov "THE RISE OF GRAPHENE"

[2] Julia A. Baimova, Sergey V. Dmitriev and Kun Zhou "Discrete breather clusters in strained graphene" EPL, 100 36005 (2012)

[3] G.Kalosakas, N. N. Lathiotakis, C.Galiotis, and K. Papagelis "In-plane force fields and elastic properties of graphene" Journal of Applied Physics 113, 134307 (2013)

[4] L. Z. Khadeeva, S. V. Dmitriev, and Yu. S. Kivshar "Discrete Breathers in Deformed Graphene" JETP LETTERS Vol. 94 No. 7 (2011)

[5] K.S.Novoselov, A. K. Geim, S.V. Morozov, D. Jiang, Y. Zhang, S. V. Dudonos, I.V.Grigorieva, A.A.Firsov "Electric Field Effect in Atomically Thin Carbon Films" Science Oct 22 (2004)

[6] R.E. Peierls "Quelques properties typiques des corpses solides" Ann. I. H. Poincare 5, 117-222 (1935)

[7] L.D. Landau "Zur Theorie der phasenumwandlungen II." Phys. Z. Sowjetunion, 11, 26-35 (1937)

[8] N. D. Mermin "Crystalline order in two dimension" Phys. Rev 176, 250-254 (1968)

[9] S. K. Singh, M. Neek-Amal, S.Costamagna and F.M. Peeters "Thermomechanical properties of a single hexagonal boron nitride sheet" Physical Review B 87, 184106 (2013)

[10] Hamidreza Akbarzadegan "An analogy between the characteristics of Carbon Nanostructures and those of Boron Nitride" Journal of Science and Engineering Vol. 2 (2), 81- 86 (2013)

[11] Masayuki Kawaguchi, Shinya Kuroda, Yasuji Muramatsu "Electronic structure and intercalation chemistry of graphite-like layered material with a composition of BC_6N" Journal of Physics and Chemisry of Solids 69 1171-1178 (2008)

[12] Martin Engler, Christoph Lesniak, Ralf Damasch, Bernd Ruisinger, Jens Eichler "Hexagonal Boron Nitride (hBN) –Applications from Metallurgy to Cosmetics" DKG 84, Vol.12 (2007)

[13] R.F. Davis "III-V Nitrides for Electronic and Optoelectronic Applications" Proceedings of the IEEE **79** (5): 702–712 (1991)

[14] L. B. Schein "Electrophotography and Development Physics" Springer Series in Electrophysics **14** (1988)

[15] N. D. Mermin and H. Wagner "Absence of Ferromagnetism or Antiferromagnetism in one or two dimentional isotropic Heisenberg Models" Physical Review Letters Vol.17 Num. 22 (1966)

[16] A. V. Savin and Y. S. Kivshar "Discrete breathers in carbon nanotubes" EPL, 82 66002 (2008)

[17] G.M. Chechin, S.V. Dmitriev, I. P. Lobzenko, D.S. Ryabov "Properties of discrete breathers in graphane from *ab initio* simulations" (2014)

[18] Y. Yamayose, Y. Kinoshita, Y. Doi, A. Nakatani and T. Kitamura "Excitation of intrinsic localized modes in a grapheme sheet" EPL, 80 40008 (2007)

[19] Daan Frenklel, Berend Smit "Understanding Molecular Simulation", Academic Press (2002)

[20] Mark E.Tuckerman, Glenn J.Martyna "Understanding Modern Molecular Dynamics: Techniques and Applications" J.Phys. Chem. B 104, 159-178 (2000)

[21] A. V. Savin, YU. S Kivshar and B. Hu, Physical Review B 82 195422 (2010)

[22] Cem Sevik, Alper Kinaci, Justin B. Haskins and Tahir Cagin "Characterization of thermal transport in low- dimensional boron nitride nanostructures" Physical Review B 84, 085409 (2011)

[23] J. Tersoff, Physical Review B 37, 6991 (1988)

[24] Steven J. Stuart, Alan B. Tutein and Judith A. Harrison "A reactive potential for hydrocarbons with intermolecular interactions" Journal of Chemical Physics Vol. 112 Num. 14 (2000)

[25] Donald W. Brenner, Olga A Shenderova, Judith A Harrison, Steven J. Stuart, Boris Ni and Susan B Sinnott "A second-generation reactive empirical bond order (REBO) potential energy expression for hydrocarbons" Journal of Physics: Condensed Matter 14, 783-802 (2002)

[26] J. H. Los and A.Fasolino "Intrinsic long-range bond-order potential for carbon: Performance in Monte Carlo simulations of graphitization" Physical Review B 68, 024107 (2003)

[27] A. Stukowski . Visualization and analysis of atomistic simulation data with OVITO - the Open Visualization Tool. Modelling Simul. Mater. Sci. Eng. 18 (2010), 015012 http://ovito.org/

[28] Compilation of L. Brewer, Lawrence Berkeley Laboratory Report No. LBL-3720

[29] A. Nag, K. Raidongia, K. P. S. S. Hembram, R. Datta, U. V. Waghmare, and C. N. R. Rao, ACS Nano **4**, 1539 (2010).

[30] D. Pacile et al, Appl. Phys. Lett. **92**, 133107 (2008)

[31] L. Lindsay, D. A. Broido. Optimized Tersoff and Brenner empirical potential parameters for lattice dynamics and phonon thermal transport in carbon nanotubes and graphene. Phys Rev B 2010